Guard cell epigenomics reveals distinct abscisic acid and CO_2 triggered chromatin remodeling during stomatal movements

Charles A. Seller and Julian I. Schroeder

School of Biological Sciences
Cell and Developmental Biology Department
University of California San Diego,
La Jolla, CA 92093-0116

*Corresponding authors. Email: cseller@ucsd.edu; jischroeder@ucsd.edu

ABSTRACT
Guard cells integrate and respond to numerous environmental signals to control stomatal pore apertures. Chromatin structure controls transcription factor access to the genome, but whether large-scale chromatin remodeling occurs in guard cells during stomatal movements, and in response to the hormone abscisic acid (ABA), remain unknown. Here we isolate guard cell nuclei from mature *Arabidopsis thaliana* plants to examine whether the physiological signals, ABA and CO_2, regulate the guard cell epigenome during stomatal movements. We reveal that ABA triggers genome-wide and persistent chromatin remodeling in guard cells, roots, and mesophyll cells. DNA motif analyses uncover binding sites for distinct transcription factors enriched in ABA-induced and ABA-repressed chromatin. We also discover bZIP transcription factors that are required for ABA-triggered chromatin opening in guard cells. We find that ABA and CO_2 induce distinct programs of chromatin remodeling. Our data support a model in which ABA-induced chromatin remodeling primes the genome for abiotic stresses.

INTRODUCTION

Organisms evolved mechanisms that connect the activity of their genome to the conditions in their environment. Developmental and environmental signals can impact the genome by regulating transcription factor (TF) binding to cognate DNA sequences known as cis-regulatory elements (CRE) (*1*). In eukaryotes, this regulation occurs in the context of chromatin where nucleosomes can impede transcription factor binding to target sequences (*2*, *3*). Consequently, the remodeling of chromatin structure to allow access of transcription factors to target DNA is thought to be a key step in gene regulation. Plant hormones are key signaling molecules controlling numerous aspects of plant life that coordinate genome activity with environmental conditions (*4*, *5*). Although recent studies have provided insight into how chromatin structure changes during plant development (*6*–*11*), it is unknown to what extent environmental and hormonal stimuli regulate chromatin accessibility.

Here we focus on the abscisic acid (ABA) signal transduction pathway to explore the connection between hormone signaling and chromatin structure in plants. ABA is a major plant stress hormone that accumulates in cells and tissues experiencing abiotic stress, especially those linked to the plant water-status (*12*–*14*). ABA signals through a well understood core module consisting of PYL/RCAR ABA receptor proteins, PP2C protein phosphatases, and SnRK2 protein kinases (*15*–*17*). ABA activates SnRK2 kinases, which in turn phosphorylate and thereby directly regulate downstream proteins including numerous transcription factors (*18*–*24*). Consequently, ABA triggers the differential expression of thousands of genes in the *Arabidopsis thaliana* genome (*4*, *25*–*27*). However, it remains unclear, especially at the genome scale, whether ABA signaling reshapes chromatin structure, and how ABA-regulated TFs might function in the context of chromatin.

One well known action of ABA is to trigger the closure of the stomatal aperture. Stomata are small pores on the surface of the leaf that mediate gas exchange and are formed by a pair of specialized epidermal cells known as guard cells. Guard cells perceive and respond to multiple environmental and hormonal cues in order to optimally regulate the size of the stomatal pore (*28*–*30*). For instance, some signals such as elevated atmospheric CO_2, ABA, and the immune elicitor Flg22 trigger stomatal closure while reduced CO_2, light and heat trigger stomatal opening. Because of their exquisite environmental reactivity, guard cells are an excellent model cell system to investigate how different signals regulate chromatin structure in a cell-type specific manner in response to physiological stimuli. Although the recent application of single-cell RNA-seq to *Arabidopsis* has expanded our understanding of gene regulation, these studies often focus on plate-grown seedlings (*31*, *32*) and/or resulted in datasets with limited representation of guard cells (*33*, *34*). To apply epigenomic techniques to the question of how guard cells respond to different stimuli new protocols are needed that can isolate large numbers of pure guard cells from soil grown plants, a more relevant setting for physiological studies.

In this paper, we describe the development of an approach to purify guard cell nuclei and by deploying this method, uncover how guard cell chromatin structure changes in response to different stimuli that drive stomatal movements. We profiled the chromatin and transcriptional reprogramming in response to ABA in three different developmental contexts – roots, mesophyll cells, and guard cells. We map thousands of loci that gain or lose chromatin accessibility in response to ABA and link these regions to co-regulated transcripts uncovering a critical role for chromatin dynamics in controlling ABA-dependent transcription. Furthermore, we show that genome-wide and persistent changes to chromatin structure accompany ABA-induced stomatal closure and that four related bZIP transcription factors known as ABRE Binding Factors (ABFs) are required for initiating the majority of ABA-induced chromatin opening. In contrast, we

implicate a family of related bHLH-type TFs known as ABA-Kinase Substrates (AKSs) in the maintenance of open chromatin upstream of ABA-repressed genes. Finally, we show that in guard cells, changes to atmospheric CO_2-concentration trigger distinct and more limited chromatin remodeling and gene regulatory programs from those mediated by abscisic acid.

RESULTS

ABA induces rapid and genome-wide chromatin remodeling in roots

As an initial test of the relationship between ABA and chromatin we focused on *Arabidopsis thaliana* seedlings. To measure changes to chromatin structure we combined fluorescence activated nuclei sorting (FANS) with the Assay for Transposase-Accessible Chromatin with sequencing (ATAC-seq), a quantitative measurement of chromatin accessibility across the genome (*35*, *36*). 50,000 nuclei per sample were isolated using FANS (Fig. S1A). We called 25,892 ATAC-seq peaks across all whole seedling libraries, genomic regions coinciding with these peaks are known as Accessible Chromatin Regions (ACRs) and predominantly aligned with upstream regulatory regions in the genome (Fig. S1B-E). In contrast, ATAC-seq reads derived from purified genomic DNA did not cluster into defined peaks (Fig. S1B,C). We first treated whole seedlings with ABA and profiled chromatin accessibility after 4 hours. Differential analysis revealed hundreds of regions that significantly gain and lose accessibility in response to ABA (Fig. 1A).

To capture the dynamics of ABA-induced chromatin remodeling we focused on roots which can rapidly take up ABA from their surroundings (*37*, *38*). Using FANS, we isolated root nuclei at three different timepoints following ABA treatment (after 45, 120, and 240 minutes) and performed ATAC-seq. Differential analysis revealed that ABA triggers time-dependent changes in chromatin accessibility in roots. Heatmaps centered over these ABA regulated ACRs illustrate the progressive impact of ABA on chromatin structure, with more regions of the genome changing in ATAC-signal over time (Fig. 1B,C). We observed significant changes to chromatin after only 45 minutes of ABA treatment, with 173 ACRs located in upstream regulatory regions gaining accessibility and 63 losing accessibility (Fig. 1C,E). After 4 hours, ABA had activated 1293 ACRs and repressed 1119 ACRs (Table S2). Interestingly, we found that ABA-regulated ACRs tend to be located more distally (> 2kb) than static regions (Fig. 1D). ABA-induced ACRs were associated with downstream genes enriched for gene ontology (GO) terms such as “response to water deprivation”, “response to osmotic stress”, and “response to abscisic acid”.

To explore the role of specific transcription factors in orchestrating these changes we performed DNA motif analysis using a set of motifs empirically generated by the in vitro DNA binding assay DAP-seq (*39*). We found that motifs recognized by ABF/AREB transcription factors such as ABF1/2/3/4 and ABI5 were highly enriched in ABA-induced ACRs (Fig. 1F, example ABF1, p = 1e-49). In contrast, we found that ABA-repressed ACRs showed enrichment for motifs recognized by the related bHLH type transcription factors AKS1, AKS3, and bHLH80 (Fig. 1F, example AKS1, p = 1e-50). Notably, both ABF1/2/3/4 and AKS1/2/3 proteins are direct targets of ABA-regulated SnRK2 kinases (*18*, *20*). Previous research has shown a role for ABA-dependent inhibition of bHLH-type AKS transcription factors in the down-regulation of the of a guard cell K^+ channel *KAT1* transcript (*20*, *40*). Interestingly, our findings suggest a larger role of the AKS clade of closely related bHLH proteins in the regulation of ABA-repressed genes. We conclude that ABA can trigger rapid and genome-wide chromatin remodeling in root tissue.

103 **Revealing guard cell specific patterns of chromatin accessibility**
104
105 Encouraged by our findings in whole seedlings and roots we next decided to investigate the
106 effect of ABA on chromatin in mature guard cells. We first developed a FACS-based strategy to
107 purify guard cell nuclei from soil-grown plants. Nuclei were labeled by expressing the histone
108 H2B fused to GFP under the control of the guard cell specific *pGC1* promoter (*41*, *42*). We first
109 confirmed the guard cell specificity of the H2B-GFP fusion in transgenic lines using fluorescence
110 microscopy (Fig. 2A). We found that chopping leaf material in lysis buffer using a razor blade
111 was insufficient to release GC nuclei, possibly due to their strong cell walls. Instead, we
112 prepared lysates by first enriching for epidermal tissue by blending the leaves of ~40 5 to 6-
113 week-old plants and then ground snap-frozen tissue using a mortar and pestle. DAPI stained
114 crude nuclei preparations were then analyzed using FACS (Fig S2A). Using this approach, we
115 could define a clearly separated GFP-positive population among all detected nuclei (Fig. 2C,
116 Fig. S2B). In contrast to many other cell types in the Arabidopsis leaf, guard cells are diploid
117 and GFP-positive nuclei from pGC1:H2B-GFP expressing plants had a 2n DNA content while
118 GFP-negative nuclei were distributed among higher ploidy levels (Fig. 2B). This method allowed
119 us to obtain ~30,000 guard cell nuclei with an estimated purity of 98% (Fig. S2C) from the
120 leaves of 40-50 plants. To assay guard cell chromatin structure, nuclei isolated using this
121 method were used to generate ATAC-seq libraries. The resulting libraries were of high quality
122 with clear concentration of peaks in annotated upstream regulatory regions (Fig. S2D),
123 enrichment of open chromatin fragments (< 100 bp) immediately upstream of transcription start
124 sites (Fig. S2E), strong correlation between biological replicates (Fig. S2F), and high FRiP
125 (fraction of reads in peaks) scores (Table S1).
126
127 In parallel, we generated ATAC-seq samples from root nuclei and from FANS-isolated
128 mesophyll nuclei labeled by expression of H2B-GFP from the promoter of the mesophyll
129 expressed Rubisco small subunit 2B gene (Fig S3A-C) (*6*). For each tissue/cell-type we
130 compared ATAC-seq libraries derived from three biological replicates. We identified 33,212
131 ATAC-seq peaks across all samples and called cell-type specific peaks using pairwise
132 differentially accessibility analysis. Although most ATAC-seq peaks were common to all cell
133 types, we found 3272 guard cell enriched ACRs, 1472 mesophyll enriched ACRs, and 3364 root
134 enriched ACRs. Heatmaps centered over these regions highlight characteristics of cell/tissue
135 specificity in the observed patterns of chromatin accessibility (Fig. 2D). Importantly, biological
136 replicates clustered together in principal component analysis with other samples derived from
137 the same tissue/cell type underscoring the robustness of this approach (Fig. 2E).
138
139 To evaluate the relationship between guard cell specific chromatin accessibility and gene
140 expression we performed RNA-seq on both whole leaves and guard cell-enriched samples. We
141 found that regions with high chromatin accessibility specifically in guard cells were associated
142 with elevated transcript levels from the adjacent downstream genes indicating that we are
143 identifying functional cis-regulatory elements (CREs) (Fig. 2F). By connecting guard cell specific
144 ACRs with downstream guard cell enriched transcripts we were able to define a set of 867
145 putative regulatory elements preferentially active in guard cells (Table S3). Examination of
146 individual gene loci like the guard cell specific genes *KAT1* (*43–45*) and *SLAC1* (*46*, *47*)
147 illustrated the connection between increased upstream accessibility and increased transcript
148 (Fig. 2G). By contrast, the mesophyll specific gene *AOC1* showed had high chromatin
149 accessibility in mesophyll cells, but minimal upstream ATAC-seq signal in guard cells. TF
150 binding motif analysis of guard cell specific ACRs returned motifs with strong similarity to known
151 guard cell transcriptional regulators such as FAMA (*48*), EDT1, and DOF (*49*) and BPC (*11*)
152 type TFs (Fig. 2H). In summary, we have developed a robust protocol for isolating pure
153 populations of guard cell nuclei allowing us to discover CREs that define guard cells.

154 **ABA induces persistent chromatin remodeling in guard cells during stomatal closure**
155
156 We next asked whether epigenomic reprogramming occurs during ABA-induced stomatal
157 closure. Soil grown 6-week-old plants were sprayed with 50 uM ABA and after 3 hours, we
158 confirmed a stomatal response by infrared photography (Fig. 3A). To determine if our ABA
159 treatment led to significant transcriptional changes we performed RNA-sequencing on both
160 whole leaf samples (Fig. S4A) and guard cell enriched samples (Fig. 3B). We observed that
161 ABA triggered the differential expression of thousands of transcripts in both whole leaves and
162 guard cells (2142 upregulated and 1574 downregulated in guard cells). As expected, ABA-
163 induced genes are enriched for the pathways “response to water deprivation” (p_value = 1.7e-
164 22), “response to abscisic acid” (pvalue = 4.47e-18), and “response to salt stress (Fig. S4D).
165 Although most of the transcriptional changes induced by ABA were shared between guard cells
166 and whole leaves, we found that 22.7% (488) of ABA-induced transcripts and 42.7% (673) of
167 ABA-repressed transcripts were specific to guard cells (Fig. S4C, Table S4). For instance, ABA
168 induced expression of the gene *HAI2* in both whole leaves and guard cells while the ABA-
169 regulated expression of the major facilitator protein-encoding *AT2G37900* and the wax
170 biosynthesis enzyme-encoding *AAE9* (*50*) were only evident in guard cells (Fig. S4E).
171
172 To evaluate if ABA changed chromatin accessibility and whether these changes are sustained
173 over time following a single treatment, we isolated guard cell nuclei at 4 hours and 24 hours
174 after spraying (Fig. 3A). We generated ATAC-seq libraries from three biological replicates per
175 time point, and PCA results showed that samples clustered together according to treatment
176 (Fig. S5A). Differential chromatin accessibility analysis found that ABA extensively reshapes
177 chromatin structure in guard cells with 2260 ACRs gaining accessibility and 1662 ACRs losing
178 accessibility across the treatment time course (Fig. 3C, Table S6). We next analyzed the
179 temporal characteristics of this response by comparing the ATAC-seq datasets from the 4-hour
180 and 24-hour timepoints. Our results allowed us to define three categories of ABA-regulated
181 ACRs – early, sustained, and late (Fig. 3D). Strikingly, we found that 1091 of the 2028 (53.8%)
182 ACRs opened by ABA at 4 hours remained open after 24 hours. Of the 990 ACRs closed by
183 ABA at 4 hours 614 (62%) remained closed at 24 hours. Additionally, we found 232 ACRs
184 gained and 670 ACRs lost accessibility only 24 hours after ABA treatment (Fig. 3D).
185
186 Consistent with our observations in seedling roots (Fig. 1D), we found that ABA-regulated
187 ATAC-seq peaks in guard cells reside further away from transcription start sites (TSS) than non-
188 regulated peaks (> 2kb), indicating that distal regulation may be a characteristic of ABA-
189 controlled CREs (Fig. S5B). ABA-induced ACRs in guard cells are clearly associated with
190 downstream genes that are upregulated transcriptionally by ABA, while ABA-repressed ACRs
191 are associated with genes downregulated by ABA (Fig. 3E). Examination of individual genes like
192 the ABA-upregulated *MYB121* and the ABA-downregulated *MYB60* (*51*) illustrate the
193 connection between upstream chromatin accessibility and transcript levels (Fig. 3F).
194 Interestingly, we found that ABA modifies chromatin accessibility upstream of many known
195 regulators of stomatal conductance including *KAT1*, *NCED3*, and *HT1* (*52*) as well as many
196 other genes with no known stomatal functions (Fig. S5C-J, Table S6).
197
198 We next performed TF binding motif analysis on these three categories of peaks using a set of
199 DAP-seq derived motifs (*39*) restricted to those TFs with guard cell expression in our RNA-seq
200 datasets. Both early and sustained ABA-induced ACRs had strong enrichment for motifs
201 recognized by ABRE- binding TFs including ABI5, ABF1,2, and 3 (Fig. 3G). Interestingly, we
202 found that the motifs recognized by CBF2, CBF3, and MYB61 (*53*–*55*) were only enriched in
203 early ABA-induced ACRs. ABA-repressed ACRs showed strong enrichment for motifs
204 recognized by a clade of related bHLH-type TFs (Fig. S5K) including AKS1, AKS3, and bHLH80

in both sustained and late categories (Fig. 3H). In contrast, MYB96 motifs were enriched only in late appearing ABA-repressed ACRs (Fig. 3H). Collectively, our results demonstrate that ABA can induce persistent changes to chromatin in guard cells and expose the temporal regulation of different TFs during this response.

By analyzing published genome-wide DAP-seq datasets (39, *56*) we found strong ABF2 DAP-seq signal coincident with ABA-induced ACRs in guard cells (Fig. 3C). Additionally, DAP-seq signals for ABF1, ABF3, and ABF4 were also enriched over regions that gain accessibility in response to ABA, although to a lesser extent than ABF2 (Fig. S5L). In contrast, ABA-repressed ACRs contained AKS1 DAP-seq binding sites (Fig. 3C). Additionally, unbiased de novo motif discovery (*57*) returned motifs similar to ABF1 and AKS3 binding sites as the most enriched in ABA-activated and ABA-repressed ACRs, respectively (p = 1e-119 and p = 1e-57). Metaplots of ATAC-seq signal centered over peaks containing these motifs further supported our observation that ABA elevates chromatin accessibility at ABF binding sites and represses chromatin accessibility at AKS binding sites (Fig. S5M). Interestingly, ABA repressed chromatin accessibility upstream of *AKS3* and decreased *AKS3* transcript levels in guard cells (Fig. 3I). To determine if AKS3 protein levels are impacted by ABA we expressed GFP tagged AKS3 under its native regulatory sequence. We observed that ABA treatment decreased GFP-AKS3 signal in guard cells (Fig. 3J).

Furthermore, by comparing ABA-induced ACRs from guard cells, mesophyll cells (Fig. S3E-G), and root cells (Fig. 1) we uncovered significant tissue/cell-type specificity in this response (Fig. 3K). Interesting, we found that ABA had a much larger impact on chromatin accessibility in guard cells than in the other cell types with more ABA regulated regions (2028 ACRs compared with 1293 in roots and 926 in mesophyll) and larger fold changes in accessibility (Tables S3,S5, and S6). In conclusion, we show that ABA drives large scale changes to chromatin structure in guard cells and implicate major roles for the activation of ABFs and inhibition of AKSs in this response.

ABF transcription factors are required for ABA-induced chromatin opening in guard cells

The mechanisms that cause ABA-specific chromatin opening are unknown. Given the strong enrichment of ABF binding motifs in ABA-activated ACRs, and their coincidence with ABF *in vitro* binding sites, we wondered if these TFs might be required for reshaping chromatin during ABA-induced stomatal closure. To test this, we used the *abf1/2/3/4* (*abfx4*) quadruple mutant which lacks four related ABF proteins that are prominent during vegetative growth (*21*, *22*). We first performed RNA-seq following ABA treatment on leaves from 6-week-old *abf1/2/3/4* (*abfx4*) mutant plants (Fig. S6A). Strikingly, of the 2469 transcripts that are upregulated by ABA in wild type leaves, 2030 (~82%) depend on ABF1/2/3/4 (Fig. S6B). Interestingly, although ABA increased *ABF1/2/3/4* transcript levels in guard cells we did not find that ABA altered chromatin accessibility in the upstream regions near the corresponding genes (Fig. S6C). We conclude that ABF1/2/3/4 are required for the bulk of ABA-induced gene expression in mature leaf tissue. Plants lacking *ABF1/2/3/4* (*abfx4*) are highly sensitive to drought stress and lose water faster than wild type plants in detached leaf assays (*22*). Consistent with this, we observed that *abfx4* mutant plants exhibited higher steady-state stomatal conductance than *Col-0* control plants (Fig. S6D).

Under non-stressed conditions, guard cells have a higher ABA concentration than other leaf cell types (*38*, *58*). Recent studies have provided evidence for basal ABA signaling in guard cells and defined important roles for basal ABA in stomatal function (*59*, *60*). By generating guard cell FANS lines in an abfx4 mutant background (Fig. S7A) we were able to assess the impact of the

loss of ABF1/2/3/4 on guard cell chromatin in non-stressed plants. In the absence of ABA treatment, we observed minimal differences in genome-wide patterns of chromatin accessibility between WT and abfx4 guard cells (Fig S7B, C) suggesting that basal ABA signaling in guard cells may regulate mainly post-transcriptional stomatal closing mechanisms, but does not significantly regulate chromatin structure.

Next, we asked if the ABF1/2/3/4 are required for the ability of ABA to reshape chromatin structure. Strikingly, loss of *abf1/2/3/4* strongly impaired ABA-induced chromatin opening in guard cells but had less impact on ABA-triggered chromatin closing (Fig. 4A). Of the 2080 ABA-induced ACRs, 1508 (~72%) required ABF1/2/3/4 for gained accessibility (Fig. 4B). As expected, ABF-dependent ACRs were strongly enriched for ABREs (p = 1e-104). Examination of individual loci including the ABA-activated genes *DTX37* and *HSFA6B* revealed a close connection between abf-dependent increases in upstream chromatin accessibility and abf-dependent transcription (Fig. 4C).

We next performed TF motif analysis on ABA-regulated accessible chromatin regions in both *WT* and *abfx4* mutant guard cells. As expected, *abfx4* mutants were depleted for ABRE motif enrichment in ABA-induced ACRs but notably retained enrichment for AKS1, AKS3, and bHLH80 motifs in ABA-repressed ACRs (Fig. 4D). Additionally, although most TF binding sites lost enrichment in ABA-induced ACRs in the absence of ABF1/2/3/4 we found that enrichment for motifs bound by CBF1, CBF2, and CBF3 was preserved. TF binding motifs are often information poor and the presence of a motif at a genomic location does not always lead to TF action. Analysis of published ABF1/2/3/4 binding assays conducted on naked genomic DNA (*56*) uncovered 11334 binding sites, but only 1315 resided within ABA-induced ACRs in guard cells (Fig. 4E). However, ABA-induced chromatin opening at these ACRs containing ABF-binding sites was strongly impaired in *abfx4* mutant guard cells (Fig. 4F). We reasoned that chromatin structure may determine which motifs are functional. To test this idea, we examined if the presence of ABF DAP-seq binding sites could predict ABA-activated transcription. By analyzing our guard cell RNA-seq data, we found that ABF binding sites that reside in regions of ABA regulated open chromatin are more strongly associated with downstream ABA-induced genes than the ABF binding sites outside of these regions (Fig. 4G).

To examine the temporal characteristics of ABF-dependent chromatin remodeling we focused on roots where ABA can reshape chromatin by 45 mins (Fig. 1C). We performed ATAC-seq on isolated *abfx4* mutant root nuclei over an ABA treatment time course and found that ABA fails to drive progressive chromatin opening in this background (Fig. S8). In *abfx4* mutant roots, 45 mins of ABA treatment induced only 6 ACRs compared to 173 in wild type roots. By 2 hours of ABA treatment, only 47 ABA-induced ACRs were present in abfx4 mutants compared with 642 in wild type (Fig. 4H and Fig. S8A). Consistent with our observations in guard cells (Fig. 4A), ABA repressed a similar number of ACRs in the absence of ABF1/2/3/4 (Fig. 4H and Fig. S8A). Collectively, these results demonstrate that the ABF1/2/3/4 transcription factors are required for triggering genome-wide chromatin opening in response to ABA.

ABA and changes to atmospheric CO_2 concentration induce distinct chromatin remodeling programs in guard cells

Because we observed that ABA has extensive effects on chromatin accessibility in guard cells, we wondered whether chromatin structure may respond to other stimuli that drive stomatal movements. Here we focus on changes to atmospheric CO_2 concentration. Exposure of plants to low CO_2 stimulates stomatal opening while high CO_2 drives stomatal closure (Fig 5A). The

307 exact role of ABA signaling during CO_2 induced stomatal responses is unclear and is a matter of
308 some debate (*59*, *61*, *60*). Recent studies suggest that although high-CO_2 induced stomatal
309 closure requires basal ABA signaling it does not involve further SnRK2 kinase activation (*59*,
310 *60*). Comparing how these signals impact genome activity could provide new insight into
311 whether and how the mechanisms underlying guard cell responses ABA and CO_2 to them may
312 differ.
313
314 To generate low and high CO_2 guard cell ATAC-seq libraries we exposed 6-week-old plants to
315 either 100 ppm CO_2 or 1000 ppm CO_2 for 4 hrs, two treatments that induce robust stomatal
316 responses (Fig 5B). Surprisingly, in contrast to the extensive effect of ABA on chromatin
317 accessibility in guard cells (Fig. 5C), we observed smaller changes in response to low CO_2 (Fig.
318 5D) and minimal changes following treatment with high CO_2 (Fig. 5E). Following exposure of
319 plants to 100 ppm CO_2, 329 ACRs gained accessibility and 487 ACRs lost accessibility while
320 treatment with 1000 ppm CO_2 induced only 11 ACRs and repressed 79 ACRs (Table S6).
321 Heatmaps of ATAC-seq signal at ABA and Low CO_2-regulated regions highlighted the specificity
322 of these responses (Fig. 5F). PCA results comparing our guard cell ATAC-seq datasets from
323 different conditions further support these findings and revealed little difference in chromatin
324 accessibility between control and high CO_2 treatments (Fig. 5G). Examination of individual loci
325 highlights the specificity of these responses, for instance chromatin opening upstream of
326 *ERF113* only occurred in response to ABA while the upstream region of the PP2C-encoding
327 *AT2G25070* gains accessibility only in response to low CO_2 (Fig. S9B-E).
328
329 Analysis of the set relationships among ABA, low CO_2, and high CO_2 regulated ACRs revealed
330 little overlap suggesting that these stimuli control distinct cis-regulatory elements in the genome
331 (Fig. S9A). We did find significant overlap between ABA-induced and low CO_2-repressed ACRs
332 and between ABA-repressed and low CO_2-induced ACRs. ABA-repressed regions had elevated
333 average ATAC-seq signal in guard cells isolated from plants exposed to 100 ppm [CO_2] (Fig.
334 5F). For instance, ABA-repressed chromatin accessibility upstream of *ALMT6* and *CBP60F*,
335 while low-CO_2 treatment enhanced accessibility (Fig. S9D,E). Interestingly, ABA repressed
336 chromatin accessibility upstream of *HT1*, *BLUS1*, and *CBC2* (*62*), all key positive regulators of
337 low CO_2- and blue light-induced stomatal opening (Fig. 5H). These data indicate that chromatin
338 remodeling represents an important cross talk point for these stimuli, ensuring robust stomatal
339 closing or opening, depending on the physiological conditions. DNA binding motif analysis
340 further emphasized the distinct regulatory impacts of changes in CO_2 concentration and ABA on
341 the genome. In contrast with ABA-induced ACRs, we did not find enrichment of ABF binding
342 motifs in low or high CO_2 regulated chromatin (Fig. 5I). Instead, low CO_2 gained ACRs were
343 enriched for motifs recognized by C2C2dof-type TFs which were oppositely enriched only in
344 ABA-repressed ACRs. Collectively, our data demonstrate how different signals that control
345 stomatal movement deploy distinct gene regulatory programs in guard cells.
346
347 DISCUSSION
348
349 Abscisic acid triggers changes in gene expression but whether this transcriptional response
350 depends on chromatin remodeling remained unknown (*5*). Here, we reveal massive ABA-
351 induced chromatin remodeling pointing to an orchestrated reprogramming of the *Arabidopsis*
352 epigenome by specific sets of transcription factors.
353
354 Guard cell regulation of stomatal aperture size is essential for plant survival under drought
355 stress. Such regulation requires that the guard cells forming the stomatal pore integrate
356 numerous physiological and environmental cues. In this study, we profiled genome-wide
357 chromatin accessibility in tens of thousands of guard cells isolated from soil-grown plants

358 exposed to different stimuli that trigger stomatal movements. Our results lead us to propose that
359 guard cell ABA signaling controls the balance between two opposing chromatin states that are
360 enforced by two major groups of transcription factors (Fig. 6). Under unstressed conditions, AKS
361 proteins maintain open chromatin at upstream regulatory regions of ABA-repressed genes while
362 ABA-activated genes are kept silent by closed chromatin. Under abiotic stress such as drought,
363 ABA levels rise in guard cells thereby activating SnRK2 kinases which subsequently inhibit
364 AKSs and activate ABFs. This would then drive the system towards a new state characterized
365 by open chromatin upstream of abiotic stress-activated genes and close chromatin upstream of
366 stress-repressed genes.
367
368 We found that ABA induces extensive and cell-type specific chromatin remodeling and that
369 guard cells possess a much more extensive response than mesophyll and root cells (Fig. 3K).
370 The plant hormone cytokinin also modulates chromatin structure (*63*) but its impact on the
371 accessible genome was smaller than what we observed for ABA (760 cytokinin-regulated ACRs
372 and 2721 ABA-regulated ACRs). By performing TF-binding motif enrichment and analyzing
373 published DAP-seq data, we hypothesized that the bZIP transcription factors ABF1/2/3/4 may
374 function in ABA-induced chromatin remodeling in guard cells (Fig. 3C,G and Fig. S5L). Our
375 experiments in *abf1/2/3/4* quadruple mutant guard cells demonstrate that these four
376 transcription factors are essential for the majority of ABA-triggered chromatin opening (Fig. 4).
377 Furthermore, experiments in root nuclei show that in *abf1/2/3/4* quadruple mutants, even early
378 ABA-induced chromatin remodeling events are strongly impaired (Fig. 4H and Fig. S8),
379 suggesting that ABFs initiate chromatin opening. How ABFs accomplish chromatin opening
380 remains to be determined, but existing literature could be interpreted to support two possible
381 and not necessarily mutually exclusive explanations. (1) Although nucleosomes can restrict TF
382 binding to DNA, some TFs, known as pioneer factors (*64*, *65*), possess the ability to bind their
383 target sequences even within inaccessible chromatin regions. At present, only a handful of
384 pioneer factors have been documented in plants (*66*), but research in mammals has shown that
385 bZIP proteins such as CEBPA can act as pioneer factors (*67*). While our data are consistent
386 with ABFs acting as pioneer factors, future biochemical experiments reconstituting ABF binding
387 to nucleosomal DNA are needed to investigate this model. (2) Additionally, ABFs may recruit
388 chromatin modifying proteins to target sequences which could increase chromatin accessibility.
389 Interestingly, several such molecules including the SWI/SNF ATPase BRM (*68*, *69*) and the
390 histone deacetylase HDA9 (*70*) interact with known ABA signaling components. Currently, no
391 direct prior evidence exists linking ABFs to chromatin remodeling or histone modifying enzymes
392 exists.
393
394 Beyond ABF1/2/3/4, our analyses implicated additional TFs in ABA-dependent genome
395 reprogramming (Fig. 3F and 3G), which correlates with prior research showing that ABA
396 regulates the binding of multiple transcription factors. We observed that ~30% of ABA-gained
397 ACRs (622 ACRs) still open in *abfx4* mutant guard cells in response to ABA (Fig. 4B). These
398 ABF-independent regions retained enrichment for CBF1/2/3 binding motifs, implicating CBF
399 transcription factors ABF-independent binding (Fig. 4D). Finally, although ABA-induced
400 chromatin opening is severely impaired in *abf1/2/3/4* quadruple mutant guard cells, we cannot
401 exclude the possibility that other ABRE-binding TFs in particular ABI5 (*71*, *72*) participate in this
402 process as well.
403
404 Notably, our data suggest that the related bHLH transcription factors AKS1/2/3 play a larger role
405 in the regulation of ABA-repressed genes than was previously thought. Prior research had
406 shown that SnRK2 kinase-dependent inhibition of AKS1/2 was required for the ABA-dependent
407 transcriptional repression of the K+ ion channel gene *KAT1* in guard cells (*20*). Surprisingly, we
408 found that AKS1 bound many regions in the genome that lose chromatin accessibility in guard

409 cells following ABA treatment (Fig. 3C). Additionally, motifs recognized by AKS1/3 and the
410 related protein bHLH80 were enriched in ABA-repressed ACRs in guard cells (Fig. 3H), as well
411 as in root and mesophyll cells (Fig. S3G). This observation was further supported by de novo
412 motif analysis (Fig S5M). AKS1 and AKS2 are inhibited by direct ABA-dependent SnRK2
413 phosphorylation, but their expression was not controlled by ABA signaling (*40*). We found that in
414 guard cells, ABA represses both AKS3 transcript and protein levels implying that ABA-
415 dependent inhibition of AKS proteins occurs through multiple mechanisms (Fig. 3I and J).
416 Together, these data point to the model that AKS TFs may play a wide-ranging role in ABA-
417 repressed transcription in diverse tissues and cell types, which will require further investigation.
418
419 Elevation in the CO_2 concentration in leaves triggers rapid stomatal closing (*30*). The extent to
420 which elevated atmospheric CO_2 signals through the ABA signal transduction pathway is
421 currently under debate. Different research groups using the same mutants have come to
422 different conclusions regarding direct CO_2 signaling via early ABA receptor/SnRK2 kinase
423 pathway during CO_2-induced stomatal closure. Our results exposed major differences in how
424 guard cells interpret these stimuli. Interestingly, in contrast to the extensive and persistent
425 changes to chromatin structure induced by ABA (Fig. 3), exposure to elevated CO_2 has minimal
426 impact on genome-wide chromatin accessibility in guard cells (Fig. 5). While ABA regulates
427 chromatin accessibility at 3018 ACRs in the genome, we found that only 90 ACRs were
428 regulated by elevated CO_2 (Fig 5C-E). Additionally, the strong enrichments of ABF binding
429 motifs in gained ACRs and AKS binding motifs in lost ACRs evident following ABA treatment are
430 absent during the response to elevated CO_2 (Fig. 5I). The disparity between these two signals at
431 the level of chromatin mirrors the disparity between characteristics of their respective
432 physiological responses. Unlike ABA- and drought-triggered stomatal closure, elevated CO_2-
433 induced stomatal closure is rapidly reversed upon return to ambient CO_2 (*59*). Such rapid
434 changes in the intercellular CO_2 concentration in leaves occur for example with alternating light
435 intensities (e.g. passing cloud cover) and require rapid reversals of stomatal CO_2 responses.
436 Furthermore, we found that exposure to low CO_2 triggers a distinct program of chromatin
437 remodeling in guard cells (Fig. 5F-I).
438
439 Finally, our results may open new avenues for investigation into two poorly understood features
440 of stomatal biology. Studies in multiple plant species have documented a phenomenon referred
441 to as stomatal "memory" (*73*, *74*). Following drought stress and re-watering, typically plants
442 exhibit delayed and/or slow re-opening of stomata despite rapid recovery of plant water status.
443 Furthermore, guard cells display transcriptional memory where repetitive dehydration stress
444 leads to altered transcript levels in subsequent stress events (*75*–*77*). This altered response can
445 exist for several days in Arabidopsis and genetic analysis showed that this response can be
446 impaired in mutants lacking key ABA-signaling components (*76*). We found that ABA triggered
447 changes to chromatin accessibility in guard cells that can persist for up to 24 hours, which could
448 prime the genome for subsequent abiotic stress exposure (Fig. 3). These shifts occurred at
449 thousands of locations in the genome including upstream of many genes known to regulate
450 stomatal movements as well as many genes with potential functions in stomatal physiology that
451 could be the basis for future studies (Fig. S5 and Table S3). Moreover, our findings support
452 crosstalk between ABA and low CO_2 signaling at the chromatin remodeling level that can
453 contribute to this stomatal memory. For example, we uncovered ABA triggered chromatin
454 closing upstream of key positive early CO_2 sensing and signaling regulators of low CO_2-induced
455 stomatal opening, including HT1 and CBC2 (Fig. 5H) (*52*, *62*)(Hashimoto et al., 2006; Hiyama et
456 al., 2017; Takahashi et al., 2022). This response may contribute to the longterm stomatal
457 closing triggered by drought and ABA, thus inhibiting mechanisms for low CO_2-induced stomatal
458 opening. ABA-triggered changes to guard cell chromatin structure provide a basis for long-term
459 reprogramming of the guard cell genome for abiotic stress survival. We envision that these

460 sustained changes to chromatin structure may store the experience of drought stress and
461 contribute to long-term adjustments of stomatal function.
462
463 METHODS
464
465 **Plant material and growth conditions**
466
467 The Columbia-0 (Col-0) accession of *Arabidopsis thaliana* was used as the wild-type
468 background. Experiments on seedlings were conducted using plants germinated and grown on
469 1/2 Murashige and Skoog (MS) media (pH 5.8) supplemented with 1% Phyto-agar plates.
470 Experiments using mature plants were conducted using plants grown in soil (Sunshine Mix #1)
471 filled plastic pots placed in a growth chamber (Conviron) under a 12hr-12hr light-dark cycle, a
472 light intensity of 100 µmol m^{-2} s^{-1}, a temperature of 22 C, ambient [CO_2], and a relative humidity
473 of 65%. To minimize the impact of environmental variation all experiments were performed on
474 plants grown in two identical growth chambers equipped with [CO_2] control.
475
476 ABA treatments in plate-based experiments were performed using a mesh (100 µm polyester)
477 transfer method to transfer seedlings in mass to treatment plates. ABA treatments on soil grown
478 plants were performed by spraying plants with 50 µM ABA (Sigma cis/trans-abscisic acid)
479 diluted with 0.01% Silwet (in water). To assess treatment responses, leaf temperature was
480 measured using an infrared thermal imaging camera (T650sc; FLIR).
481
482 **Plasmid DNA and plant transformation**
483 Constructs for cell-type specific nuclear sorting were prepared using multi-site gateway
484 technology (Invitrogen). The ORF encoding histone H2B (AT5G22880) was cloned in a
485 pDONR221 entry vector. Cell type specific promotors were cloned from the Arabidopsis genome
486 into gateway entry vectors. Final plant transformation constructs were generated by performing
487 multisite gateway recombination into the pP7m34GW destination vector. The plasmid for
488 expressing GFP-AKS3 under the AKS3 endogenous promotor was generated using GreenGate
489 cloning (*78*). The cloned AKS3 upstream regulatory sequence was defined using guard cell
490 ATAC-seq data. Primer sequences are available in Table S4. Constructs were transformed into
491 A. thaliana Col-0 plants using the floral dipping technique with *Agrobacterium tumefaciens* strain
492 GV3101.
493
494 **Microscopy**
495 Plant leaves were mounted on conventional glass microscope slides in water with the abaxial
496 epidermal layer against the coverslip. GFP fluorescence was recorded using an Eclipse
497 TE2000-U (Nikon, Tokyo, Japan) spinning disc confocal microscope. Constant gain and
498 exposure times were used for each experiment when comparing treatments/samples. Images
499 were processed for publication using Fiji software.
500
501 **Time resolved stomatal conductance measurements**
502 For gas exchange experiments, *Col-0* and *abfx4* mutant plants were grown together in the same
503 growth chamber to minimize biological variation. Intact leaves of six-week-old plants were used
504 for gas exchange experiments and stomatal conductance was measured using a Licor 6400
505 infrared gas exchange analyzer equipped with a leaf chamber (LI-COR Biosciences). Before
506 beginning measurements, clamped leaves were equilibrated for 45-60 mins at 150 µmol m^{-2} s^{-1}
507 light intensity, ~65% relative humidity, 21ºC, 400 ppm [CO_2], and an air flow of 400 µmol s^{-1}.
508 Stomatal conductance was recorded every 30 seconds for a total of 30 min. To control for the
509 effect of the diurnal rhythm on stomatal physiology, gas exchange experiments began 2 hr after
510 the beginning of the light cycle and measurements were made alternating between different

genotypes. Data are presented as average stomatal conductance +/- standard error of 4 plants per genotype.

Fluorescence-activated nuclear sorting (FANS)

FANS was performed similar to (*36*) with small modifications. For experiments on seedlings, approximately 200 whole seedlings or whole roots severed with a scalpel were collected, transferred to a glass petri dish containing 2 ml of pre-chilled FANS-lysis buffer (15 mM Tris-HCl pH7.5, 20 mM NaCl, 80 mM KCl, 0.5 mM spermine, 1 mM spermidine, 5 mM 2-ME, 0.2% TritonX-100, 1 Pierce mini EDTA-free protease inhibitor cocktail), and chopped with a clean razor blade for 4 mins. Lysates were filtered through a 40 µm filter before transferring to new 15 ml tubes containing 4 ml of FANS-Sucrose buffer (20 mM Tris-HCl Ph8.0, 2 mM $MgCl_2$, 2 mM EDTAl, 15 mM 2-ME, 1.7 M sucrose, 0.2% TritonX-100). Nuclei were pelleted by centrifugation at 2200xg at 4C for 20 mins. The crude nuclei pellet was resuspended in 600 µl of FANS-lysis buffer supplemented with 4,6-Diamidino-2-phenylindole (DAPI).

For experiments on guard cells, the leaves of ~40 six-week-old plants were harvested and blended in 500 ml of ice-cold water for 2x30 secs with 1 min between pulses. The blended sample was then poured over a 100 µm mesh to remove mesophyll cells and collect epidermal enriched fragments. The mesh was gently rinsed with ~200 ml of water and after gently removing excess liquid, the thin sections of the collected epidermal tissue were flash-frozen in liquid nitrogen. Epidermal sections were ground in a frozen mortar and pestle to a fine powder. After grinding, powder was transferred to a new mortar with a frozen metal. Immediately 12 ml of ice-cold FANS-lysis buffer was added, and the powder was gently resuspended with a clean pestle. The subsequent lysate was filtered through a 40 µm filter unit before transferring to a 15 ml tube containing 6 ml of FANS-Sucrose buffer. Nuclei were collected as above, before resuspending in 600 µl FANS-lysis buffer supplemented with DAPI.

Flow cytometry was conducted on a BD FACS Aria II using a 70 µm nozzle with a flow rate < 2 and the following photomultiplier tube parameters: FSC – 250 eV, SSC – 220 eV, BV421 – 550 eV, FITC – 340 eV. Sort gates were defined empirically to exclude debris and potential doublets. Before sorting GFP labeled nuclei, FACS analysis on unlabeled control samples was performed to define background signal. Sorted nuclei were collected in 600 µl of FANS-lysis buffer in a refrigerated tube chamber. Sort gates After sorting, nuclei were pelleted by centrifugation at 1000xg for 10 mins at 4C. Nuclei pellets were gently washed with 1 ml of 10 mM Tris-HCl pH8.0, 5 mM MgCl2 buffer, before centrifugation again as above. After carefully removing the supernatant, nuclei were used for ATAC-seq.

RNA-seq

For whole leaf RNA-seq, total RNA was extracted from the leaves from 6 plants per sample using the Spectrum total RNA isolation kit. For guard cell enriched RNA-seq, the leaves of 20 plants per sample were blended for 30 sec in ice-cold water, filtered through a 100 µm mesh, and then blended and filtered again as above to isolate epidermal tissue. Total RNA was then extracted using the Qiagen RNeasy mini kit. mRNA-seq libraries were prepared and sequenced on a NovaSeq 6000 (PE100) at the UCSD Institute for Genomic Medicine.

Following sequencing, adapter trimming and quality control checks were performed using Trim Galore version 0.6.5 (Cutadapt and FastQC). Reads were aligned to the Arabidopsis genome (TAIR10) by Rsubread version 2.14.0 (*79*). Low quality aligments (mapping quality < 2) were removed using Samtools view function version 1.17 (*80*). Read count per transcript matrices were generated using Rsubread featureCounts. Differential expression analysis was performed using DESeq2 version 1.26.0 (*81*). Transcripts were defined as significantly differentially

562 expressed using the following thresholds: P adjusted value < 0.001 and fold change > 2. To
563 visualize data using the Integrated Genome Browser (IGV), bigwig coverage tracks were
564 generated using deepTools (version 3.5.0) bamCoverage function with a bin size of 1 bp and
565 normalization using RPKM (*82*). Gene ontology (GO) term enrichment analysis was done using
566 the Panther system (*83*).
567
568 **ATAC-seq**
569 ATAC-seq was performed as described in (*84*). Sorted nuclei were resuspended in 40 µl of
570 tagmentation reaction mixture (20 µl 2xTD buffer, 0.4 µl 10% Tween, 0.4 µl 1% digitonin, 13.2 µl
571 1xPBS, X µl H2O) supplemented with TDE1 enzyme (Illumina) at a ratio of 2.0 µl TDE1:50,000
572 nuclei. Reactions were incubated at 37C for 30 mins. Tagmented DNA fragments were purified
573 using the Qiagen min-Elute DNA kit. ATAC-seq libraries were amplified with dual indexed
574 primers using the NEBNext 2xHiFi PCR Master Mix (New England Biolabs) for 5 initial cycles.
575 The number of additional amplification cycles was determined empirically by performing qPCR
576 on 10% of the amplified library. Amplified libraries dual size selected using a 0.6x-1.2X ratio of
577 SPRIselect magnetic beads (Beckman Coulter). ATAC-seq libraries were pooled and
578 sequenced on a NovaSeq 6000 (PE150 mode) by Novogene.
579
580 To control for differences in data analysis between studies, previously published Mesophyll cell
581 ATAC-seq raw FASTQ files were downloaded from SRA (SRP113667) and reanalyzed.
582 Following sequencing, adapter trimming and quality control checks were performed using Trim
583 Galore version 0.6.5 (Cutadapt and FastQC). Parallel processing was performed using GNU
584 Parallel (*85*). Reads were aligned to the *Arabidopsis* genome (TAIR10) by Rsubread version
585 2.14.0. Low quality aligments (mapping quality < 2) and alignments to the mitochondrial and
586 chloroplast genomes were removed using Samtools view function version 1.17. Alignments in a
587 region of chromosome 2 (3239001 – 3510171) with abnormally high ATAC-seq signal in all
588 samples were removed prior to further processing using bedtools version 2.30. Duplicated reads
589 were filtered using Picard tools Markduplicates version 1.141. ATAC-seq peaks were called
590 across all biological replicated using Genrich (*86*) with the following parameters: -r -d -j -p 0.01 -
591 a 200. ATAC-seq peaks were then merged across all samples using bedtools merge function to
592 generate a master list of peaks. ATAC-seq reads were then assigned to peaks using
593 featureCounts and Fragments in peaks scores (FRiPs) were calculated. Differential chromatin
594 accessibility analysis was performed using DESeq2 version 1.26.0. Regions were defined as
595 significantly differentially accessible using the following thresholds: P adjusted value < 0.001
596 and fold change > 1.5 or 2 as indicated in associated figure legends. To visualize data using the
597 Integrated Genome Browser (IGV), bigwig coverage tracks were generated on merged replicate
598 bam files using deepTools (version 3.5.0) bamCoverage function with a bin size of 1 bp and
599 normalization using RPKM. Peaks were assigned to nearest downstream gene (within 2 kb) by
600 ChipSeeker (version 1.8.6) function seq2gene (*87*). Gene ontology (GO) term enrichment
601 analysis was done using the Panther system. Heatmaps and metaplots of z score-normalized
602 read depth were generated with DeepTools. Homer software (version 2.1.2) (*57*) was used to
603 for de novo motif discovery for differentially accessible ATAC peaks and to match discovered
604 motifs to previously known motifs from databases. We used ChIPpeakAnno software (Version
605 3.24) (*88*) to assign ATAC-seq peaks to annotated genomic features and to test for genomic
606 overlap among different sets of peaks.
607
608 **DAP-seq Analysis**
609 To control for differences in data analysis between studies, previously published DAP-seq
610 datasets GSE60143 (*39*) and PRJNA682697 (*56*) were reanalyzed. Raw FASTQ files were
611 downloaded from SRA and processed to remove adapters using Trim Galore. Reads were
612 aligned to the Arabidopsis genome using Rsubread and low quality aligments (mapping quality

< 2) were removed using the Samtools view function. DAP-seq peaks were called using MACS2 (version 2.2.7). For ABF1/2/3/4 DAP-seq datasets, peaks were merged across four replicate experiments. Bigwig files were generated on merged replicate DAP-seq bam files using deepTools (version 3.5.0) bamCoverage function with a bin size of 1 bp and normalization via RPKM. DeepTools software was used to generate heatmaps and Metaprofile plots centered over ABA-regulated ACRs

ACKNOWLEDGEMENTS

This research was supported by National Institutes of Health grant R01GM060396 to J.I.S. and by National Institutes of Health Ruth L. Kirschstein National Research Service Awards Postdoctoral Fellowship 5F32GM137544 to C.A.S. Experiments on CO_2 responses were supported by National Science Foundation grant NSF MCB-1900567 to J.I.S. This publication includes data generated at the UC San Diego IGM Genomics Center utilizing an Illumina NovaSeq 6000 that was purchased with funding from a National Institutes of Health SIG grant (#S10 OD026929). We thank Kazuko Yamaguchi-Shinozaki (University of Tokyo) for sharing *abf1/2/3/4* quadruple mutant seeds, and members of the Schroeder lab for helpful discussions thoughout the research.

AUTHOR CONTRIBUTIONS

C.A.S. and J.I.S. conceived and designed the research. C.A.S. conducted all experiments and performed data analysis. C.A.S. and J.I.S. wrote and edited the manuscript.

FIGURE LEGENDS

Figure 1. ABA induced rapid and genome-wide chromatin remodeling in seedlings. A) Volcano plot of differential ATACseq analysis showing regions that significantly change in chromatin accessibility in seedlings after 4hrs of ABA treatment. ABA increased accessibility at 744 regions and decreased accessibility at 257 regions (FDR < 0.001 and FC > 1.5). **B)** Heatmap of root nuclei ATAC-seq signal at regions showing ABA-regulated chromatin accessibility over the indicated ABA treatment time course. Across all timepoints, ABA increased accessibility at 1293 regions and decreased accessibility at 1119 regions (FDR < 0.001 and FC > 1.5). **C)** Number of ABA-regulated ATAC-seq peaks over time in roots. Bars summarizing ABA-induced peaks are colored in blue while bars representing ABA-repressed peaks are colored in pink. **D)** Genomic distribution among annotated features of all ATAC-seq peaks (orange) and in ABA-regulated ATAC-seq peaks (grey). **E)** Genome browser snapshots at two representative genes (*MAPKKK18* and CML25) showing changes in ATAC-seq signal in upstream regions following ABA treatment. **F)** The transcription factor binding motifs with the highest enrichment (by binomial p-value) in ABA-induced and ABA-repressed chromatin regions in roots.

Fig 2. Cell-type specific epigenomics identifies guard cell specific regulatory elements. A) Fluorescence micrograph showing guard cell specific expression of H2B-GFP. **B)** DAPI density plot shows that GFP positive nuclei (blue population) are diploid, while GFP negative nuclei (pink population) are distributed over multiple ploidies. **C)** FACS analysis of nuclei (DAPI positive) from *GC1:H2b-GFP* plants. GFP density plot defines two distinct populations separated by GFP intensity. **D)** Chromatin accessibility heatmaps comparing ATAC-seq samples derived from guard cell, mesophyll, or root cell nuclei. ATAC-seq peaks are separated into guard cell enriched (3272 ACRs), mesophyll enriched (1472 ACRs), and root enriched (3364 ACRs) sets defined by differential accessibility (p.adj < 0.001, FoldChange > 2). **E)**

Principal component analysis (PCA) comparing ATAC-seq biological replicates derived from guard cell, mesophyll, or root nuclei. Samples clustered by tissue/cell-type of origin. **F)** ATAC-seq and RNA-seq metaplots showing average chromatin accessibility at guard cell specific peaks and average transcript levels of the nearest downstream gene (within 2 kb). Guard cell derived signal is shown in black while mesophyll/leaf signal is shown in green. **G)** Genome browser comparing ATAC-seq and RNA-seq signal for the indicated tracks at three example loci: two guard cell specific – *KAT1* and *SLAC1*, and one mesophyll cell specific gene – *AOC1*. **H)** Results of de novo motif analysis using homer. The top four most enriched motifs (by binomial p-value) are shown along with the best matching known TFs and associated p-value.

Figure 3. ABA triggers extensive and persistent chromatin remodeling in guard cells. A) Schematic showing the experimental outline. Plants were sprayed with ABA and infrared images were taken using a thermal camera to assess stomatal closure. Guard cell nuclei were purified at 4hrs and 24 hrs after treatment and used for ATAC-seq. **B)** Volcano plot of guard cell enriched RNA-seq data showing ABA upregulates 2134 transcripts and downregulates 1452 transcripts (FDR < 0.001, FC > 2.0). **C)** Heatmaps and profile plots of ATAC-seq signal in guard cell nuclei centered over 2260 regions with ABA-induced chromatin accessibility and 1662 regions with ABA-repressed chromatin accessibility (FDR < 0.001, FC > 2.0). The adjacent heatmaps show DAP-seq signal for ABF2 (in red) and AKS1 (in black) at the same ABA regulated ACRs, data from (39) and (56). **D)** Comparison of ABA-regulated peaks from 4hr and 24hr after treatment separated regions into three categories – early only, sustained (both early and late), and late only. The bar graph shows the number of ABA-increased and -decreased regions in each category. **E)** ATAC-seq and RNA-seq metaplots showing average chromatin accessibility and transcript levels near ABA-induced and ABA-repressed ATAC-seq peaks. **F)** Genome browser images showing guard cell ATAC-seq and RNA-seq coverage at a representative ABA-induced gene (*MYB121)* and an ABA-repressed gene (*MYB60*). **G,H)** Heatmaps showing TF binding site enrichment (-log(p-value)) in ABA-increased **(G)** and ABA-decreased **(H)** ATAC-seq peaks. **I)** Genome browser images showing guard cell ATAC-seq and RNA-seq coverage near the *AKS3* gene. **J)** Fluorescence micrograph showing expression of *AKS3pr::GFP-AKS3* in guard cells after treatment with control or ABA (4 hr). **K)** Overlap of ABA-induced accessible regions in guard cell nuclei, mesophyll nuclei, and root nuclei.

Fig 4. ABF transcription factors are required for ABA-induced chromatin opening in guard cells. A) Heatmaps of ATAC-seq signal in either *WT* or *abfx4* mutant guard cells at 2029 regions with ABA-induced accessibility subdivided by dependency for ABF1/2/3/4 and 991 regions with ABA-repressed accessibility (FDR < 0.001 and FC > 2.0). **B)** Overlap of ABA-induced ATAC-seq peaks in *WT* guard cells with those in *abfx4* mutant guard cells. **C)** Genome browser snapshots showing ATAC-seq and RNA-seq signal near two ABA-induced genes *DTX37* and *HSFA6B*. **D)** Enrichment (-log P_value) of the indicated transcription factor binding motifs in ABA regulated ATAC-seq peaks in either *WT* or *abfx4* mutant guard cell nuclei. Negative enrichment scores indicate motifs overrepresented in condition-repressed regions. **E)** Overlap between ABF DAP-seq peaks and ABA-induced accessible chromatin regions (ACRs). **F)** Peak-centered metaplot showing ATAC-seq signal in the indicated samples at ABA-induced ATAC-seq peaks containing ABF DAP-seq binding sites. **G)** 1000 ABF-DAP-seq peaks overlapping ABA-induced ATAC-seq peaks or 1000 random ABF DAP-seq binding sites were assigned to nearest upstream genes. The plot shows the percentage of these genes that are transcriptionally induced by ABA treatment. **H)** Bar plots representing the number of ABA-activated or ABA-repressed ACRs over time in *Col-0* or *abfx4* mutant roots.

Fig 5. ABA and changes in CO_2 concentration induce distinct chromatin remodeling programs in guard cells. A) Diagram showing the effects of different stimuli on the stomatal

715 aperture. **B)** Representative IR image showing differences in leaf temperature due to CO_2
716 induced stomatal movement. **C-E)** Volcano plots of ATAC-seq data showing **C)** ABA-regulated
717 chromatin accessibility, **D)** low CO_2 regulated chromatin accessibility, and **E)** high CO2
718 regulated chromatin accessibility. The number of differentially accessible peaks (colored in red,
719 FDR < 0.001 and FC > 2.0) in each condition is indicated on each plot. **F)** Heatmaps and profile
720 plots of guard cell ATAC-seq signal centered over either ABA-regulated ACRs (2028 induced
721 and 991 repressed) or low CO_2-regulated ACRs (329 induced and 487 repressed). Libraries are
722 derived from plants exposed to the indicated treatments. **G)** Principal component analysis (PCA)
723 shows that ABA, low CO_2, and high CO_2 introduce separate variation to genome-wide chromatin
724 accessibility. **H)** Genome browser snapshots showing ABA-repression of chromatin accessibility
725 upstream of HT1, BLUS1, and CBC1 – three positive regulators of low CO_2 induced stomatal
726 opening. **I)** Enrichment (-log P_value) of the indicated transcription factor binding motifs in ABA,
727 Low CO_2, or High CO_2 regulated regions. Negative enrichment scores indicate motifs
728 overrepresented in condition-repressed regions.
729
730 **Fig. 6 Model - ABA regulates opposing chromatin states in guard cells.** In unstressed
731 guard cells, AKS proteins maintain open chromatin at ABA-repressed genes while ABA-induced
732 genes are kept silent by closed chromatin at their upstream regulatory regions. During abiotic
733 stress, SnRK2s activate ABFs and inhibit AKSs. This leads to the establishment of open
734 chromatin at stress-activated genes and the silencing of ABA-repressed genes by the closing of
735 chromatin. Graphic created with Biorender.com.
736
737 **SUPPLEMENTAL CAPTIONS**
738
739 **Fig. S1. FANS-ATACseq on seedling nuclei reproducibly assays chromatin accessibility**
740 **in regulatory DNA. A)** Density plot DAPI fluorescence shows the distribution of ploidy among
741 FACS-sorted nuclei from seedlings. **B)** Open chromatin reads (<100 bp) of a seedling ATAC-
742 seq library shows strong enrichment upstream of transcription start sites (TSSs). **C)** Genome
743 browser snapshot of a region of chromosome 1 showing ATACseq signal derived from either
744 50,000 seedling nuclei (two replicates shown in blue) or from purified genomic DNA (in pink). **D)**
745 Scatterplot of ATAC-seq coverage showing correlation between two ATAC-seq replicates. **E)**
746 Genomic distribution of seedling nuclei ATAC-seq peaks among annotated features.
747
748 **Fig S2. Guard cell FANS-ATAC-seq. A)** Diagram of the protocol used to isolate guard cell
749 nuclei from *Arabidopsis* plants. The leaves of roughly 40 6-week-old GC1:H2b-GFP plants were
750 blended in ice cold water. The resulting blendate was filtered through a 100 um mesh sheet to
751 isolate epidermal tissue. A representative fluorescence micrograph shows intact guard cells with
752 nuclei labeled by H2b-GFP. Epidermal tissue was flash frozen in LN2 and then ground to a fine
753 powder using a mortar and pestle. After extracting nuclei from ground tissue, GFP positive
754 nuclei were purified using FACS. **B)** DAPI vs GFP intensity plot resulting from FACS analysis of
755 nuclei (DAPI positive) from *GC1:H2b-GFP* plants (in green) and *Col-0* plants (in black). **C)**
756 Sorted guard cell nuclei were re-run through the same FACS protocol to evaluate the purity of
757 the isolated population. The DAPI vs GFP plot shows nuclei passing (green) and failing (black)
758 the sorting criteria. Out of 10,000 sorted nuclei, 9821 passed (purity of 98%). **D)** Pie chart
759 displaying the distribution of guard cell ATAC-seq peaks among annotated genomic features are
760 colored in green while nuclei that failed GFP density plot defines two distinct populations
761 separated by GFP intensity. **E)** TSS enrichment plot of open chromatin reads (<100 bp) from a
762 Guard Cell ATAC-seq library shows strong enrichment upstream of transcription start sites
763 (TSSs). **F)** Scatterplots showing the correlation among biological replicates of guard cell ATAC-
764 seq libraries.
765

Figure S3. ABA induced chromatin remodeling in mesophyll cell nuclei. A) GFP vs DAPI intensity plot showing the results of FACS analysis on nuclei from *RBCp::H2b-GFP* plants. The location of GFP positive mesophyll nuclei sorted for ATAC-seq is indicated dashed box. Inset shows a confocal image showing the expression of *RBCp::H2b-GFP* in mesophyll cell nuclei. **B)** ATAC-seq coverage plot showing strong enrichment of mesophyll ATAC-seq reads upstream of Transcription Start Sites (TSSs). **C)** Overlap of mesophyll ATAC-seq peaks from (*6*) with those from this study. **D)** Representative IR image showing increase in leaf surface temperature 3hrs after spraying *RBC:H2b-GFP* plants with ABA. **E)** Heatmap of ATAC-seq signal in mesophyll nuclei at regions showing ABA-regulated chromatin accessibility. ABA significantly increased accessibility at 926 regions and decreased accessibility at 436 regions (FDR < 0.001 and FC > 1.5). **F)** Genome browser snapshots at representative genes (*MAPKKK18* and HB12) showing ABA-regulated chromatin accessibility in upstream sequences. **G)** Selection of transcription factor binding motifs enriched in ABA-induced and ABA-repressed ATAC-seq regions in mesophyll nuclei.

Fig S4. RNA-seq identifies ABA-regulated transcripts in guard cells and wholeleaf tissue. A) Volcano plot of differential RNA-seq analysis (FDR < 0.001, FC > 2) comparing control and ABA-treated samples from both whole leaf and guard cells. Differentially expressed transcripts are colored in red (2316 upregulated and 1529 downregulated). **B)** Principal component analysis (PCA) of RNA-seq results showing samples clustering by treatment (ABA vs control) and cell-type (guard cell vs leaf). **C)** Overlap of transcripts induced or repressed by ABA between whole leaves and guard cells. **D)** Results of a Gene Ontology (GO) analysis performed on ABA-induced transcripts. **E)** Genome browser snapshots showing RNA-seq signal from the indicated samples at the representative ABA-regulated genes *HAI2, AT2G37900,* and *AAE9*.

Fig. S5. ABA triggered chromatin remodeling in guard cells. A) PCA plot of guard cell ATAC-seq samples from ABA treatment experiment. **B)** Genomic distribution among annotated features of guard cell ATAC-seq peaks separated into regions that are static (black) and those that are ABA-regulated (orange). **C-J)** Additional examples of ABA-induced changes to chromatin accessibility upstream of **C)** *HT1* which encodes a kinase controlling low CO_2 induced stomatal opening, **D)** the ABA-activated kinase *MAPKKK18*, **E)** ABA biosynthesis gene *NCED3*, **F)** the wax biosynthesis gene *AAE9*, **G)** *RD29B*, **H)** the aquaporin *PIP1;4*, **I)** *LTP4*, and **J)** the cell wall expansin gene *EXPA1*. **K)** Cladogram generated from multiple sequence alignment (ClustalW) of related *Arabidopsis* bHLH transcription factors. TFs with motifs enriched in ABA-repressed ACRs are highlighted in green. **L)** Metaprofile plots of DAP-seq signal for ABF1/2/3/4 centered over ABA-induced or ABA-repressed ACRs. **M)** De novo motif discovery uncovered motifs similar to ABF1 and AKS3 in ABA-activated and ABA-repressed ACRs, respectively. Metaplots of control and ABA-treated guard cell ATAC-seq samples centered over peaks containing either of these motifs are shown below the indicated DNA motifs.

Fig S6. The ABRE binding proteins ABF1-4 are required for the bulk of ABA-induced transcription in mature leaf tissue. A) Volcano plot of RNA-seq results from ABA or control treated 5-week old *abfx4* mutant leaf tissue. ABA significantly upregulated 561 transcripts and downregulated 724 transcripts (FDR < 0.001 and FC > 2). **B)** Overlap of ABA-induced transcripts in *Col-0* leaves vs *abfx4* mutant leaves shows that ABFs are required for the upregulation of 2030 transcripts. **C)** Genome browser snapshots showing guard cell ATAC-seq signal and RNA-seq signal 4 genes encoding ABFs. Chromatin accessibility upstream of *ABF1-4* was not significantly increased by ABA in guard cells. **D)** Gas exchange (Licor-6400) comparing steady state stomatal conductance of well-watered Col-0 and abfx4 plants (n = 5 per genotype).

817 **Fig S7. Chromatin accessibility in *abfx4* mutant guard cells without ABA treatment. A)**
818 Confocal image showing guard cell specific expression of H2B-GFP in *abfx4* mutant leaf. **B)**
819 Principal component analysis (PCA) of Guard cell ATAC-seq results showing samples clustering
820 by treatment (ABA vs control) and genotype (*Col-0* vs *abfx4*). **C)** Volcano plot summarizing
821 differential ATAC-seq analysis (FDR < 0.001 and FC > 2.0) comparing chromatin accessibility in
822 control treated *WT* vs *abfx4* mutant guard cells.
823
824 **Fig S8. ABFs are required for ABA-induced chromatin opening in roots. A)** Heatmap of
825 ATAC-seq signal at regions showing ABA-regulated chromatin accessibility over the indicated
826 ABA treatment time course in either *WT* or *abfx4* mutant root nuclei. **B)** Principal component
827 analysis of root ATAC-seq libraries showing separation of samples by both genotype and ABA
828 treatment duration. **C)** Genome browser snapshot showing chromatin accessibility in *WT* or
829 *abfx4* mutant root nuclei upstream of the ABA-induced gene *MAPKKK18* over the indicated ABA
830 treatment time series.
831
832 **Fig S9. Distinct regulation of chromatin by ABA and CO_2 in guard cells. A)** UpSet plot
833 showing the set relationships between ABA, low CO_2, and high CO_2 regulated ATAC-seq peaks.
834 Overlapping sets are indicated by the filled in circles below the bar graph and the number of
835 peaks contained within the set is labeled above the respective bar. **B-E)** Genome browser
836 images showing ABA and CO_2-regulated chromatin accessibility upstream of **B)** *ERF113*, **C)**
837 *AT2G25070*, **D)** *ALMT6*, and **E)** *CBP60F*.
838
839 **Supplementary tables**
840 Table S1. Summary of sequencing libraries.
841 Table S2. ABA-regulated accessible chromatin regions in roots.
842 Table S3. High confidence guard cell specific cis-regulatory regions.
843 Table S4. ABA-regulated transcripts in whole leaves and guard cells.
844 Table S5. ABA-regulated accessible chromatin regions in mesophyll cells.
845 Table S6. ABA- and [CO_2]-regulated accessible chromatin regions in guard cells.

REFERENCES

1. R. J. Schmitz, E. Grotewold, M. Stam, Cis-regulatory sequences in plants: Their importance, discovery, and future challenges. *The Plant Cell*. **34**, 718–741 (2022).

2. W. K. M. Lai, B. F. Pugh, Understanding nucleosome dynamics and their links to gene expression and DNA replication. *Nature Reviews Molecular Cell Biology*. **18**, 548–562 (2017).

3. T. C. Voss, G. L. Hager, Dynamic regulation of transcriptional states by chromatin and transcription factors. *Nature Reviews Genetics*. **15**, 69–81 (2014).

4. J. L. Nemhauser, F. Hong, J. Chory, Different Plant Hormones Regulate Similar Processes through Largely Nonoverlapping Transcriptional Responses. *Cell*. **126**, 467–475 (2006).

5. R. Waadt, C. A. Seller, P.-K. Hsu, Y. Takahashi, S. Munemasa, J. I. Schroeder, Plant hormone regulation of abiotic stress responses. *Nat Rev Mol Cell Biol*. **23**, 680–694 (2022).

6. P. Sijacic, M. Bajic, E. C. McKinney, R. B. Meagher, R. B. Deal, Changes in chromatin accessibility between Arabidopsis stem cells and mesophyll cells illuminate cell type-specific transcription factor networks. *The Plant Journal*. **94**, 215–231 (2018).

7. K. A. Maher, M. Bajic, K. Kajala, M. Reynoso, G. Pauluzzi, D. A. West, K. Zumstein, M. Woodhouse, K. Bubb, M. W. Dorrity, C. Queitsch, J. Bailey-Serres, N. Sinha, S. M. Brady, R. B. Deal, Profiling of Accessible Chromatin Regions across Multiple Plant Species and Cell Types Reveals Common Gene Regulatory Principles and New Control Modules. *The Plant Cell*. **30**, 15–36 (2018).

8. A. Farmer, S. Thibivilliers, K. H. Ryu, J. Schiefelbein, M. Libault, Single-nucleus RNA and ATAC sequencing reveals the impact of chromatin accessibility on gene expression in Arabidopsis roots at the single-cell level. *Molecular Plant*. **14**, 372–383 (2021).

9. M. Borg, R. K. Papareddy, R. Dombey, E. Axelsson, M. D. Nodine, D. Twell, F. Berger, Epigenetic reprogramming rewires transcription during the alternation of generations in Arabidopsis. *eLife*. **10**, e61894 (2021).

10. A. P. Marand, Z. Chen, A. Gallavotti, R. J. Schmitz, A cis-regulatory atlas in maize at single-cell resolution. *Cell*. **184**, 3041-3055.e21 (2021).

11. E.-D. Kim, M. W. Dorrity, B. A. Fitzgerald, H. Seo, K. M. Sepuru, C. Queitsch, N. Mitsuda, S.-K. Han, K. U. Torii, Dynamic chromatin accessibility deploys heterotypic cis/trans-acting factors driving stomatal cell-fate commitment. *Nat. Plants*. **8**, 1453–1466 (2022).

12. S. R. Cutler, P. L. Rodriguez, R. R. Finkelstein, S. R. Abrams, Abscisic Acid: Emergence of a Core Signaling Network. *Annual Review of Plant Biology*. **61**, 651–679 (2010).

13. R. Finkelstein, Abscisic Acid Synthesis and Response. *Arabidopsis Book*. **11** (2013), doi:10.1199/tab.0166.

14. J.-K. Zhu, Abiotic Stress Signaling and Responses in Plants. *Cell*. **167**, 313–324 (2016).

15. Y. Ma, I. Szostkiewicz, A. Korte, D. Moes, Y. Yang, A. Christmann, E. Grill, Regulators of PP2C Phosphatase Activity Function as Abscisic Acid Sensors. *Science*. **324**, 1064–1068 (2009).

16. S.-Y. Park, P. Fung, N. Nishimura, D. R. Jensen, H. Fujii, Y. Zhao, S. Lumba, J. Santiago, A. Rodrigues, T. F. Chow, S. E. Alfred, D. Bonetta, R. Finkelstein, N. J. Provart, D. Desveaux, P. L. Rodriguez, P. McCourt, J.-K. Zhu, J. I. Schroeder, B. F. Volkman, S. R. Cutler, Abscisic Acid Inhibits Type 2C Protein Phosphatases via the PYR/PYL Family of START Proteins. *Science*. **324**, 1068–1071 (2009).

17. T. Umezawa, N. Sugiyama, M. Mizoguchi, S. Hayashi, F. Myouga, K. Yamaguchi-Shinozaki, Y. Ishihama, T. Hirayama, K. Shinozaki, Type 2C protein phosphatases directly regulate abscisic acid-activated protein kinases in Arabidopsis. *Proceedings of the National Academy of Sciences*. **106**, 17588–17593 (2009).

18. H. Fujii, P. E. Verslues, J.-K. Zhu, Identification of Two Protein Kinases Required for Abscisic Acid Regulation of Seed Germination, Root Growth, and Gene Expression in Arabidopsis. *The Plant Cell*. **19**, 485–494 (2007).

19. K. E. Hubbard, N. Nishimura, K. Hitomi, E. D. Getzoff, J. I. Schroeder, Early abscisic acid signal transduction mechanisms: newly discovered components and newly emerging questions. *Genes Dev.* **24**, 1695–1708 (2010).

20. Y. Takahashi, Y. Ebisu, T. Kinoshita, M. Doi, E. Okuma, Y. Murata, K. Shimazaki, bHLH Transcription Factors That Facilitate K+ Uptake During Stomatal Opening Are Repressed by Abscisic Acid Through Phosphorylation. *Science Signaling*. **6**, ra48–ra48 (2013).

21. T. Yoshida, Y. Fujita, H. Sayama, S. Kidokoro, K. Maruyama, J. Mizoi, K. Shinozaki, K. Yamaguchi-Shinozaki, AREB1, AREB2, and ABF3 are master transcription factors that cooperatively regulate ABRE-dependent ABA signaling involved in drought stress tolerance and require ABA for full activation. *The Plant Journal*. **61**, 672–685 (2010).

22. T. Yoshida, Y. Fujita, K. Maruyama, J. Mogami, D. Todaka, K. Shinozaki, K. Yamaguchi-Shinozaki, Four Arabidopsis AREB/ABF transcription factors function predominantly in gene expression downstream of SnRK2 kinases in abscisic acid signalling in response to osmotic stress. *Plant, Cell & Environment*. **38**, 35–49 (2015).

23. P. Wang, L. Xue, G. Batelli, S. Lee, Y.-J. Hou, M. J. V. Oosten, H. Zhang, W. A. Tao, J.-K. Zhu, Quantitative phosphoproteomics identifies SnRK2 protein kinase substrates and reveals the effectors of abscisic acid action. *PNAS*. **110**, 11205–11210 (2013).

24. T. Umezawa, N. Sugiyama, F. Takahashi, J. C. Anderson, Y. Ishihama, S. C. Peck, K. Shinozaki, Genetics and Phosphoproteomics Reveal a Protein Phosphorylation Network in the Abscisic Acid Signaling Pathway in Arabidopsis thaliana. *Sci. Signal.* **6**, rs8–rs8 (2013).

25. N. Leonhardt, J. M. Kwak, N. Robert, D. Waner, G. Leonhardt, J. I. Schroeder, Microarray Expression Analyses of Arabidopsis Guard Cells and Isolation of a Recessive Abscisic Acid Hypersensitive Protein Phosphatase 2C Mutant. *The Plant Cell*. **16**, 596–615 (2004).

26. H. Goda, E. Sasaki, K. Akiyama, A. Maruyama-Nakashita, K. Nakabayashi, W. Li, M. Ogawa, Y. Yamauchi, J. Preston, K. Aoki, T. Kiba, S. Takatsuto, S. Fujioka, T. Asami, T.

Nakano, H. Kato, T. Mizuno, H. Sakakibara, S. Yamaguchi, E. Nambara, Y. Kamiya, H. Takahashi, M. Y. Hirai, T. Sakurai, K. Shinozaki, K. Saito, S. Yoshida, Y. Shimada, The AtGenExpress hormone and chemical treatment data set: experimental design, data evaluation, model data analysis and data access. *The Plant Journal*. **55**, 526–542 (2008).

27. R.-S. Wang, S. Pandey, S. Li, T. E. Gookin, Z. Zhao, R. Albert, S. M. Assmann, Common and unique elements of the ABA-regulated transcriptome of Arabidopsis guard cells. *BMC Genomics*. **12**, 216 (2011).

28. A. M. Hetherington, F. I. Woodward, The role of stomata in sensing and driving environmental change. *Nature*. **424**, 901–908 (2003).

29. S. M. Assmann, T. Jegla, Guard cell sensory systems: recent insights on stomatal responses to light, abscisic acid, and CO2. *Current Opinion in Plant Biology*. **33**, 157–167 (2016).

30. G. Dubeaux, P.-K. Hsu, P. H. O. Ceciliato, K. J. Swink, W.-J. Rappel, J. I. Schroeder, Deep dive into CO2-dependent molecular mechanisms driving stomatal responses in plants. *Plant Physiology*. **187**, 2032–2042 (2021).

31. Z. Liu, Y. Zhou, J. Guo, J. Li, Z. Tian, Z. Zhu, J. Wang, R. Wu, B. Zhang, Y. Hu, Y. Sun, Y. Shangguan, W. Li, T. Li, Y. Hu, C. Guo, J.-D. Rochaix, Y. Miao, X. Sun, Global Dynamic Molecular Profiling of Stomatal Lineage Cell Development by Single-Cell RNA Sequencing. *Molecular Plant*. **13**, 1178–1193 (2020).

32. C. B. Lopez-Anido, A. Vatén, N. K. Smoot, N. Sharma, V. Guo, Y. Gong, M. X. Anleu Gil, A. K. Weimer, D. C. Bergmann, Single-cell resolution of lineage trajectories in the Arabidopsis stomatal lineage and developing leaf. *Developmental Cell*. **56**, 1043-1055.e4 (2021).

33. J.-Y. Kim, E. Symeonidi, T. Y. Pang, T. Denyer, D. Weidauer, M. Bezrutczyk, M. Miras, N. Zöllner, T. Hartwig, M. M. Wudick, M. Lercher, L.-Q. Chen, M. C. P. Timmermans, W. B. Frommer, Distinct identities of leaf phloem cells revealed by single cell transcriptomics. *The Plant Cell*. **33**, 511–530 (2021).

34. C. Procko, T. Lee, A. Borsuk, B. O. R. Bargmann, T. Dabi, J. R. Nery, M. Estelle, L. Baird, C. O'Connor, C. Brodersen, J. R. Ecker, J. Chory, Leaf cell-specific and single-cell transcriptional profiling reveals a role for the palisade layer in UV light protection. *The Plant Cell*. **34**, 3261–3279 (2022).

35. J. D. Buenrostro, P. G. Giresi, L. C. Zaba, H. Y. Chang, W. J. Greenleaf, Transposition of native chromatin for fast and sensitive epigenomic profiling of open chromatin, DNA-binding proteins and nucleosome position. *Nature Methods*. **10**, 1213–1218 (2013).

36. Z. Lu, B. T. Hofmeister, C. Vollmers, R. M. DuBois, R. J. Schmitz, Combining ATAC-seq with nuclei sorting for discovery of cis-regulatory regions in plant genomes. *Nucleic Acids Research*. **45**, e41 (2017).

37. A. M. Jones, J. Å. Danielson, S. N. ManojKumar, V. Lanquar, G. Grossmann, W. B. Frommer, Abscisic acid dynamics in roots detected with genetically encoded FRET sensors. *eLife*. **3**, e01741 (2014).

38. R. Waadt, K. Hitomi, N. Nishimura, C. Hitomi, S. R. Adams, E. D. Getzoff, J. I. Schroeder, FRET-based reporters for the direct visualization of abscisic acid concentration changes and distribution in Arabidopsis. *eLife*. **3**, e01739 (2014).

39. R. C. O'Malley, S. C. Huang, L. Song, M. G. Lewsey, A. Bartlett, J. R. Nery, M. Galli, A. Gallavotti, J. R. Ecker, Cistrome and Epicistrome Features Shape the Regulatory DNA Landscape. *Cell*. **165**, 1280–1292 (2016).

40. Y. Takahashi, T. Kinoshita, M. Matsumoto, K. Shimazaki, Inhibition of the Arabidopsis bHLH transcription factor by monomerization through abscisic acid-induced phosphorylation. *The Plant Journal*. **87**, 559–567 (2016).

41. Y. Yang, A. Costa, N. Leonhardt, R. S. Siegel, J. I. Schroeder, Isolation of a strong Arabidopsis guard cell promoter and its potential as a research tool. *Plant Methods*. **4**, 6 (2008).

42. M. M. Marquès-Bueno, A. K. Morao, A. Cayrel, M. P. Platre, M. Barberon, E. Caillieux, V. Colot, Y. Jaillais, F. Roudier, G. Vert, A versatile Multisite Gateway-compatible promoter and transgenic line collection for cell type-specific functional genomics in Arabidopsis. *The Plant Journal*. **85**, 320–333 (2016).

43. J. A. Anderson, S. S. Huprikar, L. V. Kochian, W. J. Lucas, R. F. Gaber, Functional expression of a probable Arabidopsis thaliana potassium channel in Saccharomyces cerevisiae. *Proceedings of the National Academy of Sciences*. **89**, 3736–3740 (1992).

44. D. P. Schachtman, J. 1. Schroeder, W. J. Lucas, J. A. Anderson, R. F. Gaber, Expression of an Inward-Rectifying Potassium Channel by the Arabidopsis KAT1 cDNA. *Science*. **258**, 1654–1658 (1992).

45. R. L. Nakamura, W. L. McKendree Jr, R. E. Hirsch, J. C. Sedbrook, R. F. Gaber, M. R. Sussman, Expression of an Arabidopsis Potassium Channel Gene in Guard Cells. *Plant Physiology*. **109**, 371–374 (1995).

46. J. Negi, O. Matsuda, T. Nagasawa, Y. Oba, H. Takahashi, M. Kawai-Yamada, H. Uchimiya, M. Hashimoto, K. Iba, CO2 regulator SLAC1 and its homologues are essential for anion homeostasis in plant cells. *Nature*. **452**, 483–486 (2008).

47. T. Vahisalu, H. Kollist, Y.-F. Wang, N. Nishimura, W.-Y. Chan, G. Valerio, A. Lamminmäki, M. Brosché, H. Moldau, R. Desikan, J. I. Schroeder, J. Kangasjärvi, SLAC1 is required for plant guard cell S-type anion channel function in stomatal signalling. *Nature*. **452**, 487–491 (2008).

48. K. Ohashi-Ito, D. C. Bergmann, Arabidopsis FAMA Controls the Final Proliferation/Differentiation Switch during Stomatal Development. *The Plant Cell*. **18**, 2493–2505 (2006).

49. J. Negi, K. Moriwaki, M. Konishi, R. Yokoyama, T. Nakano, K. Kusumi, M. Hashimoto-Sugimoto, J. I. Schroeder, K. Nishitani, S. Yanagisawa, K. Iba, A Dof Transcription Factor, SCAP1, Is Essential for the Development of Functional Stomata in Arabidopsis. *Current Biology*. **23**, 479–484 (2013).

50. S. Li, X. Yang, H. Huang, R. Qiao, M. A. Jenks, H. Zhao, S. Lü, Arabidopsis ACYL-ACTIVATING ENZYME 9 (AAE9) encoding an isobutyl-CoA synthetase is a key factor connecting branched-chain amino acid catabolism with iso-branched wax biosynthesis. *New Phytologist*. **233**, 2458–2470 (2022).

51. E. Cominelli, M. Galbiati, A. Vavasseur, L. Conti, T. Sala, M. Vuylsteke, N. Leonhardt, S. L. Dellaporta, C. Tonelli, A Guard-Cell-Specific MYB Transcription Factor Regulates Stomatal Movements and Plant Drought Tolerance. *Current Biology*. **15**, 1196–1200 (2005).

52. M. Hashimoto, J. Negi, J. Young, M. Israelsson, J. I. Schroeder, K. Iba, Arabidopsis HT1 kinase controls stomatal movements in response to CO2. *Nat Cell Biol*. **8**, 391–397 (2006).

53. Y.-K. Liang, C. Dubos, I. C. Dodd, G. H. Holroyd, A. M. Hetherington, M. M. Campbell, AtMYB61, an R2R3-MYB Transcription Factor Controlling Stomatal Aperture in Arabidopsis thaliana. *Current Biology*. **15**, 1201–1206 (2005).

54. M. B. Prouse, M. M. Campbell, Interactions between the R2R3-MYB Transcription Factor, AtMYB61, and Target DNA Binding Sites. *PLOS ONE*. **8**, e65132 (2013).

55. S. J. Gilmour, D. G. Zarka, E. J. Stockinger, M. P. Salazar, J. M. Houghton, M. F. Thomashow, Low temperature regulation of the Arabidopsis CBF family of AP2 transcriptional activators as an early step in cold-induced COR gene expression. *The Plant Journal*. **16**, 433–442 (1998).

56. Y. Sun, D.-H. Oh, L. Duan, P. Ramachandran, A. Ramirez, A. Bartlett, K.-N. Tran, G. Wang, M. Dassanayake, J. R. Dinneny, Divergence in the ABA gene regulatory network underlies differential growth control. *Nat. Plants*, 1–12 (2022).

57. S. Heinz, C. Benner, N. Spann, E. Bertolino, Y. C. Lin, P. Laslo, J. X. Cheng, C. Murre, H. Singh, C. K. Glass, Simple Combinations of Lineage-Determining Transcription Factors Prime cis-Regulatory Elements Required for Macrophage and B Cell Identities. *Molecular Cell*. **38**, 576–589 (2010).

58. W. Lahr, K. Raschke, Abscisic-acid contents and concentrations in protoplasts from guard cells and mesophyll cells ofVicia faba L. *Planta*. **173**, 528–531 (1988).

59. P.-K. Hsu, Y. Takahashi, S. Munemasa, E. Merilo, K. Laanemets, R. Waadt, D. Pater, H. Kollist, J. I. Schroeder, Abscisic acid-independent stomatal CO2 signal transduction pathway and convergence of CO2 and ABA signaling downstream of OST1 kinase. *Proceedings of the National Academy of Sciences*. **115**, E9971–E9980 (2018).

60. L. Zhang, Y. Takahashi, P.-K. Hsu, H. Kollist, E. Merilo, P. J. Krysan, J. I. Schroeder, FRET kinase sensor development reveals SnRK2/OST1 activation by ABA but not by MeJA and high CO2 during stomatal closure. *eLife*. **9**, e56351 (2020).

61. M. Dittrich, H. M. Mueller, H. Bauer, M. Peirats-Llobet, P. L. Rodriguez, C.-M. Geilfus, S. C. Carpentier, K. A. S. Al Rasheid, H. Kollist, E. Merilo, J. Herrmann, T. Müller, P. Ache, A. M. Hetherington, R. Hedrich, The role of Arabidopsis ABA receptors from the PYR/PYL/RCAR family in stomatal acclimation and closure signal integration. *Nat. Plants*. **5**, 1002–1011 (2019).

62. A. Hiyama, A. Takemiya, S. Munemasa, E. Okuma, N. Sugiyama, Y. Tada, Y. Murata, K. Shimazaki, Blue light and CO2 signals converge to regulate light-induced stomatal opening. *Nat Commun*. **8**, 1284 (2017).

63. K. C. Potter, J. Wang, G. E. Schaller, J. J. Kieber, Cytokinin modulates context-dependent chromatin accessibility through the type-B response regulators. *Nature Plants*. **4**, 1102–1111 (2018).

64. M. Iwafuchi-Doi, K. S. Zaret, Pioneer transcription factors in cell reprogramming. *Genes Dev.* **28**, 2679–2692 (2014).

65. A. Balsalobre, J. Drouin, Pioneer factors as master regulators of the epigenome and cell fate. *Nat Rev Mol Cell Biol*, 1–16 (2022).

66. R. Jin, S. Klasfeld, Y. Zhu, M. Fernandez Garcia, J. Xiao, S.-K. Han, A. Konkol, D. Wagner, LEAFY is a pioneer transcription factor and licenses cell reprogramming to floral fate. *Nat Commun*. **12**, 626 (2021).

67. C. van Oevelen, S. Collombet, G. Vicent, M. Hoogenkamp, C. Lepoivre, A. Badeaux, L. Bussmann, J. L. Sardina, D. Thieffry, M. Beato, Y. Shi, C. Bonifer, T. Graf, C/EBPα Activates Pre-existing and De Novo Macrophage Enhancers during Induced Pre-B Cell Transdifferentiation and Myelopoiesis. *Stem Cell Reports*. **5**, 232–247 (2015).

68. S.-K. Han, Y. Sang, A. Rodrigues, B. F2010, M.-F. Wu, P. L. Rodriguez, D. Wagner, The SWI2/SNF2 Chromatin Remodeling ATPase BRAHMA Represses Abscisic Acid Responses in the Absence of the Stress Stimulus in Arabidopsis. *The Plant Cell*. **24**, 4892–4906 (2012).

69. M. Peirats-Llobet, S.-K. Han, M. Gonzalez-Guzman, C. W. Jeong, L. Rodriguez, B. Belda-Palazon, D. Wagner, P. L. Rodriguez, A Direct Link between Abscisic Acid Sensing and the Chromatin-Remodeling ATPase BRAHMA via Core ABA Signaling Pathway Components. *Molecular Plant*. **9**, 136–147 (2016).

70. D. Baek, G. Shin, M. C. Kim, M. Shen, S. Y. Lee, D.-J. Yun, Histone Deacetylase HDA9 With ABI4 Contributes to Abscisic Acid Homeostasis in Drought Stress Response. *Frontiers in Plant Science*. **11** (2020) (available at https://www.frontiersin.org/articles/10.3389/fpls.2020.00143).

71. R. Finkelstein, S. S. L. Gampala, T. J. Lynch, T. L. Thomas, C. D. Rock, Redundant and Distinct Functions of the ABA Response Loci ABA-INSENSITIVE(ABI)5 and ABRE-BINDING FACTOR (ABF)3. *Plant Mol Biol*. **59**, 253–267 (2005).

72. R. R. Finkelstein, T. J. Lynch, The Arabidopsis Abscisic Acid Response Gene ABI5 Encodes a Basic Leucine Zipper Transcription Factor. *The Plant Cell*. **12**, 599–609 (2000).

73. E. Fleta-Soriano, M. Pintó-Marijuan, S. Munné-Bosch, Evidence of Drought Stress Memory in the Facultative CAM, Aptenia cordifolia: Possible Role of Phytohormones. *PLOS ONE*. **10**, e0135391 (2015).

74. P. A. Auler, F. B. S. Freire, V. F. Lima, D. M. Daloso, On the role of guard cells in sensing environmental signals and memorising stress periods. *Theor. Exp. Plant Physiol.* **34**, 277–299 (2022).

75. Y. Ding, M. Fromm, Z. Avramova, Multiple exposures to drought "train" transcriptional responses in *Arabidopsis*. *Nature Communications*. **3**, 740 (2012).

76. L. Virlouvet, M. Fromm, Physiological and transcriptional memory in guard cells during repetitive dehydration stress. *New Phytologist*. **205**, 596–607 (2015).

77. A. van Weringh, A. Pasha, E. Esteban, P. J. Gamueda, N. J. Provart, Generation of guard cell RNA-seq transcriptomes during progressive drought and recovery using an adapted INTACT protocol for Arabidopsis thaliana shoot tissue (2021), p. 2021.04.15.439991, , doi:10.1101/2021.04.15.439991.

78. A. Lampropoulos, Z. Sutikovic, C. Wenzl, I. Maegele, J. U. Lohmann, J. Forner, GreenGate - A Novel, Versatile, and Efficient Cloning System for Plant Transgenesis. *PLOS ONE*. **8**, e83043 (2013).

79. Y. Liao, G. K. Smyth, W. Shi, The R package Rsubread is easier, faster, cheaper and better for alignment and quantification of RNA sequencing reads. *Nucleic Acids Research*. **47**, e47 (2019).

80. H. Li, B. Handsaker, A. Wysoker, T. Fennell, J. Ruan, N. Homer, G. Marth, G. Abecasis, R. Durbin, 1000 Genome Project Data Processing Subgroup, The Sequence Alignment/Map format and SAMtools. *Bioinformatics*. **25**, 2078–2079 (2009).

81. M. I. Love, W. Huber, S. Anders, Moderated estimation of fold change and dispersion for RNA-seq data with DESeq2. *Genome Biology*. **15**, 550 (2014).

82. F. Ramírez, D. P. Ryan, B. Grüning, V. Bhardwaj, F. Kilpert, A. S. Richter, S. Heyne, F. Dündar, T. Manke, deepTools2: a next generation web server for deep-sequencing data analysis. *Nucleic Acids Research*. **44**, W160–W165 (2016).

83. H. Mi, A. Muruganujan, D. Ebert, X. Huang, P. D. Thomas, PANTHER version 14: more genomes, a new PANTHER GO-slim and improvements in enrichment analysis tools. *Nucleic Acids Research*. **47**, D419–D426 (2019).

84. J. Buenrostro, B. Wu, H. Chang, W. Greenleaf, *Curr Protoc Mol Biol*, in press, doi:10.1002/0471142727.mb2129s109.

85. O. Tange, GNU Parallel 20220922 ('Elizabeth'). *Zenodo* (2022), doi:10.5281/zenodo.7105792.

86. J. M. Gaspar, Genrich: detecting sites of genomic enrichment (2021), (available at https://github.com/jsh58/Genrich#readme).

87. G. Yu, L.-G. Wang, Q.-Y. He, ChIPseeker: an R/Bioconductor package for ChIP peak annotation, comparison and visualization. *Bioinformatics*. **31**, 2382–2383 (2015).

88. L. J. Zhu, C. Gazin, N. D. Lawson, H. Pagès, S. M. Lin, D. S. Lapointe, M. R. Green, ChIPpeakAnno: a Bioconductor package to annotate ChIP-seq and ChIP-chip data. *BMC Bioinformatics*. **11**, 237 (2010).

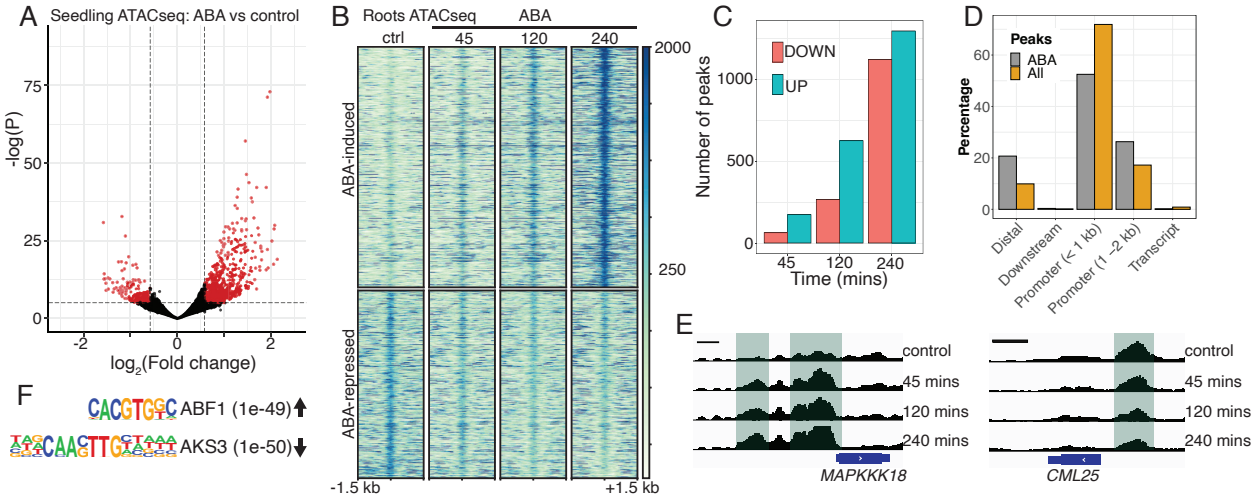

Figure 1. ABA induced rapid and genome-wide chromatin remodeling in seedlings. A) Volcano plot of differential ATACseq analysis showing regions that significantly change in chromatin accessibility in seedlings after 4hrs of ABA treatment. ABA increased accessibility at 744 regions and decreased accessibility at 257 regions (FDR < 0.001 and FC > 1.5). **B)** Heatmap of root nuclei ATAC-seq signal at regions showing ABA-regulated chromatin accessibility over the indicated ABA treatment time course. Across all timepoints, ABA increased accessibility at 1293 regions and decreased accessibility at 1119 regions (FDR < 0.001 and FC > 1.5). **C)** Number of ABA-regulated ATAC-seq peaks over time in roots. Bars summarizing ABA-induced peaks are colored in blue while bars representing ABA-repressed peaks are colored in pink. **D)** Genomic distribution among annotated features of all ATAC-seq peaks (orange) and in ABA-regulated ATAC-seq peaks (grey). **E)** Genome browser snapshots at two representative genes (*MAPKKK18* and CML25) showing changes in ATAC-seq signal in upstream regions following ABA treatment. **F)** The transcription factor binding motifs with the highest enrichment (by binomial p-value) in ABA-induced and ABA-repressed chromatin regions in roots.

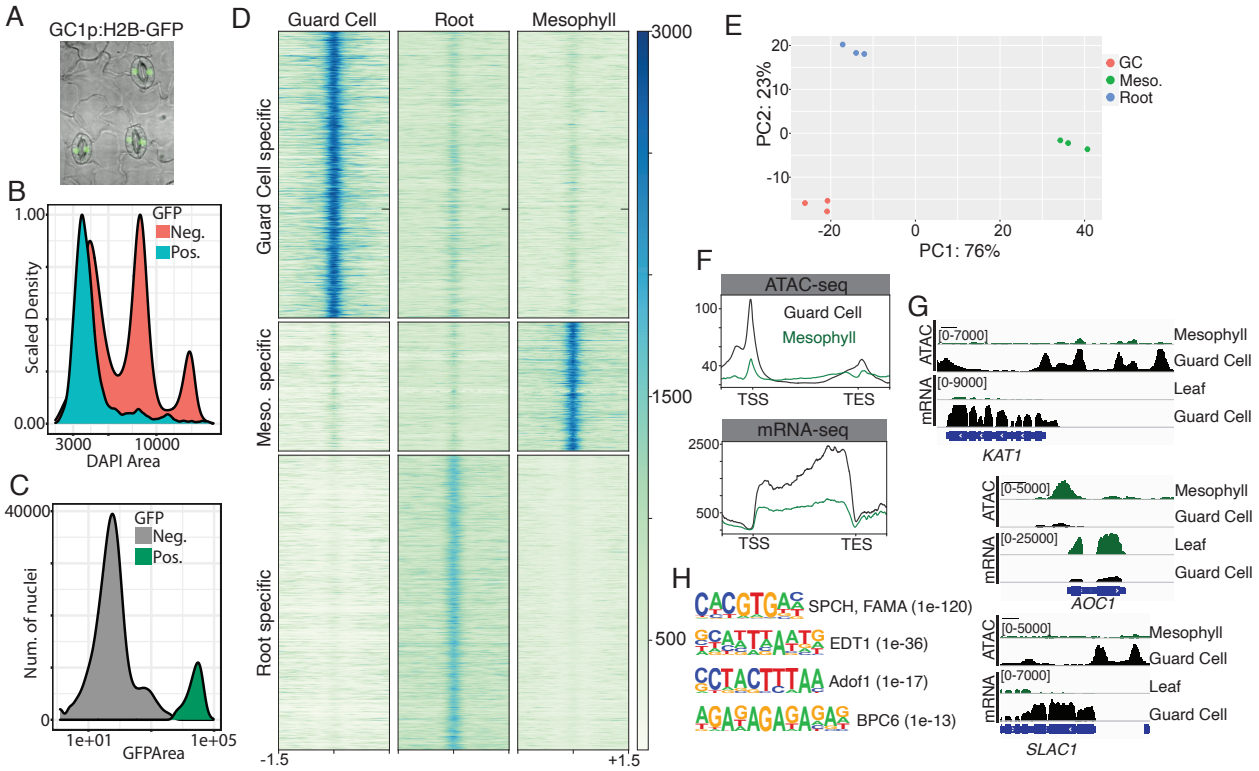

Fig 2. Cell-type specific epigenomics identifies guard cell specific regulatory elements. A) Fluorescence micrograph showing guard cell specific expression of H2B-GFP. **B)** DAPI density plot shows that GFP positive nuclei (blue population) are diploid, while GFP negative nuclei (pink population) are distributed over multiple ploidies. **C)** FACS analysis of nuclei (DAPI positive) from *GC1:H2b-GFP* plants. GFP density plot defines two distinct populations separated by GFP intensity. **D)** Chromatin accessibility heatmaps comparing ATAC-seq samples derived from guard cell, mesophyll, or root cell nuclei. ATAC-seq peaks are separated into guard cell enriched (3272 ACRs), mesophyll enriched (1472 ACRs), and root enriched (3364 ACRs) sets defined by differential accessibility (p.adj < 0.001, FoldChange > 2). **E)** Principal component analysis (PCA) comparing ATAC-seq biological replicates derived from guard cell, mesophyll, or root nuclei. Samples clustered by tissue/cell-type of origin. **F)** ATAC-seq and RNA-seq metaplots showing average chromatin accessibility at guard cell specific peaks and average transcript levels of the nearest downstream gene (within 2 kb). Guard cell derived signal is shown in black while mesophyll/leaf signal is shown in green. **G)** Genome browser comparing ATAC-seq and RNA-seq signal for the indicated tracks at three example loci: two guard cell specific – *KAT1* and *SLAC1*, and one mesophyll cell specific gene – *AOC1*. **H)** Results of de novo motif analysis using homer. The top four most enriched motifs (by binomial p-value) are shown along with the best matching known TFs and associated p-value.

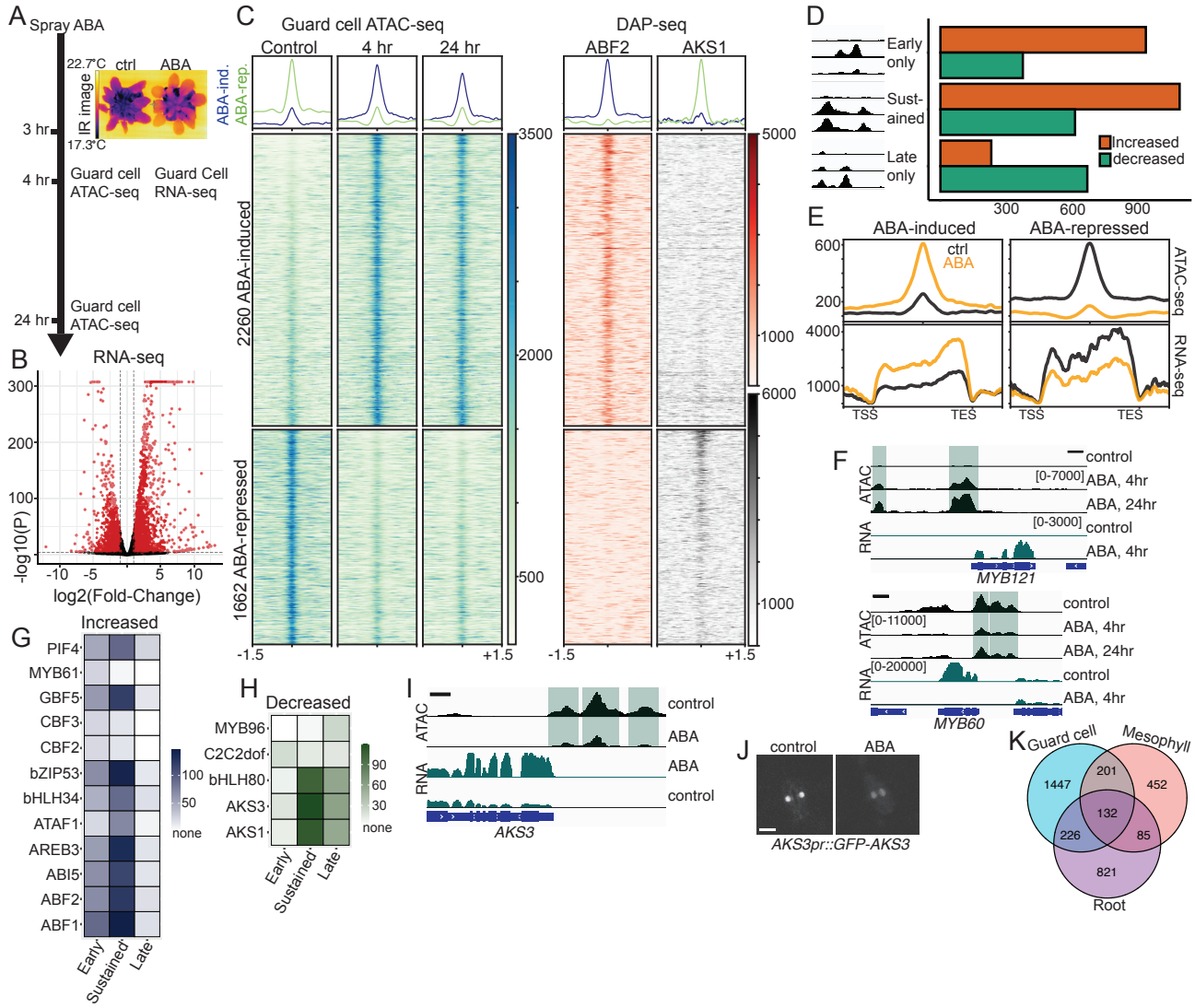

Figure 3. ABA triggers extensive and persistent chromatin remodeling in guard cells. **A)** Schematic showing the experimental outline. Plants were sprayed with ABA and infrared images were taken using a thermal camera to assess stomatal closure. Guard cell nuclei were purified at 4hrs and 24 hrs after treatment and used for ATAC-seq. **B)** Volcano plot of guard cell enriched RNA-seq data showing ABA upregulates 2134 transcripts and downregulates 1452 transcripts (FDR < 0.001, FC > 2.0). **C)** Heatmaps and profile plots of ATAC-seq signal in guard cell nuclei centered over 2260 regions with ABA-induced chromatin accessibility and 1662 regions with ABA-repressed chromatin accessibility (FDR < 0.001, FC > 2.0). The adjacent heatmaps show DAP-seq signal for ABF2 (in red) and AKS1 (in black) at the same ABA regulated ACRs, data from (39) and (56). **D)** Comparison of ABA-regulated peaks from 4hr and 24hr after treatment separated regions into three categories – early only, sustained (both early and late), and late only. The bar graph shows the number of ABA-increased and -decreased regions in each category. **E)** ATAC-seq and RNA-seq metaplots showing average chromatin accessibility and transcript levels near ABA-induced and ABA-repressed ATAC-seq peaks. **F)** Genome browser images showing guard cell ATAC-seq and RNA-seq coverage at a representative ABA-induced gene (*MYB121)* and an ABA-repressed gene (*MYB60*). **G,H)** Heatmaps showing TF binding site enrichment (-log(p-value)) in ABA-increased **(G)** and ABA-decreased **(H)** ATAC-seq peaks. **I)** Genome browser images showing guard cell ATAC-seq and

RNA-seq coverage near the *AKS3* gene. **J)** Fluorescence micrograph showing expression of *AKS3pr::GFP-AKS3* in guard cells after treatment with control or ABA (4 hr). **K)** Overlap of ABA-induced accessible regions in guard cell nuclei, mesophyll nuclei, and root nuclei.

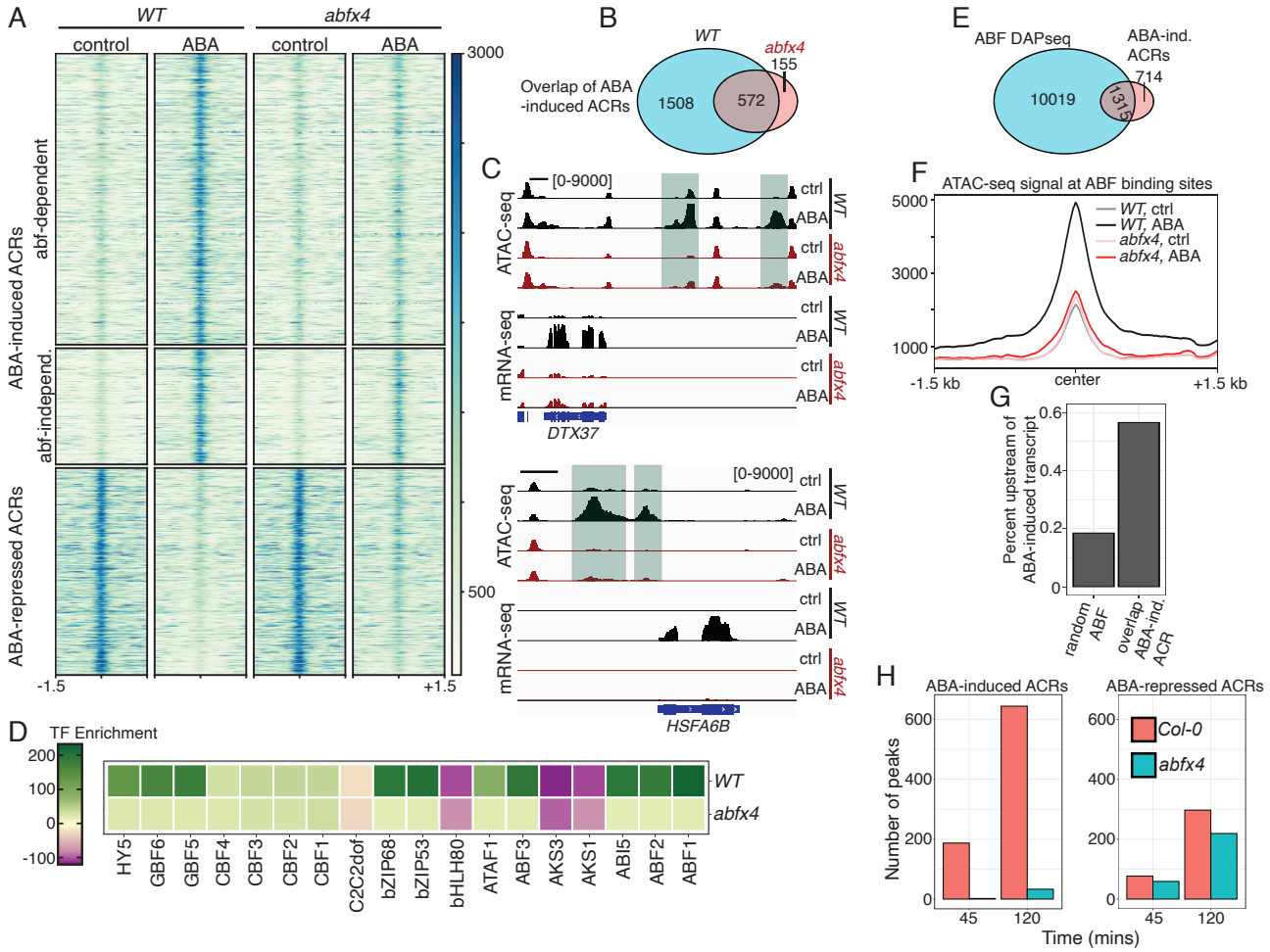

Fig 4. ABF transcription factors are required for ABA-induced chromatin opening in guard cells. A) Heatmaps of ATAC-seq signal in either *WT* or *abfx4* mutant guard cells at 2029 regions with ABA-induced accessibility subdivided by dependency for ABF1/2/3/4 and 991 regions with ABA-repressed accessibility (FDR < 0.001 and FC > 2.0). **B)** Overlap of ABA-induced ATAC-seq peaks in *WT* guard cells with those in *abfx4* mutant guard cells. **C)** Genome browser snapshots showing ATAC-seq and RNA-seq signal near two ABA-induced genes *DTX37* and *HSFA6B*. **D)** Enrichment (-log P_value) of the indicated transcription factor binding motifs in ABA regulated ATAC-seq peaks in either *WT* or *abfx4* mutant guard cell nuclei. Negative enrichment scores indicate motifs overrepresented in condition-repressed regions. **E)** Overlap between ABF DAP-seq peaks and ABA-induced accessible chromatin regions (ACRs). **F)** Peak-centered metaplot showing ATAC-seq signal in the indicated samples at ABA-induced ATAC-seq peaks containing ABF DAP-seq binding sites. **G)** 1000 ABF-DAP-seq peaks overlapping ABA-induced ATAC-seq peaks or 1000 random ABF DAP-seq binding sites were assigned to nearest upstream genes. The plot shows the percentage of these genes that are transcriptionally induced by ABA treatment. **H)** Bar plots representing the number of ABA-activated or ABA-repressed ACRs over time in *Col-0* or *abfx4* mutant roots.

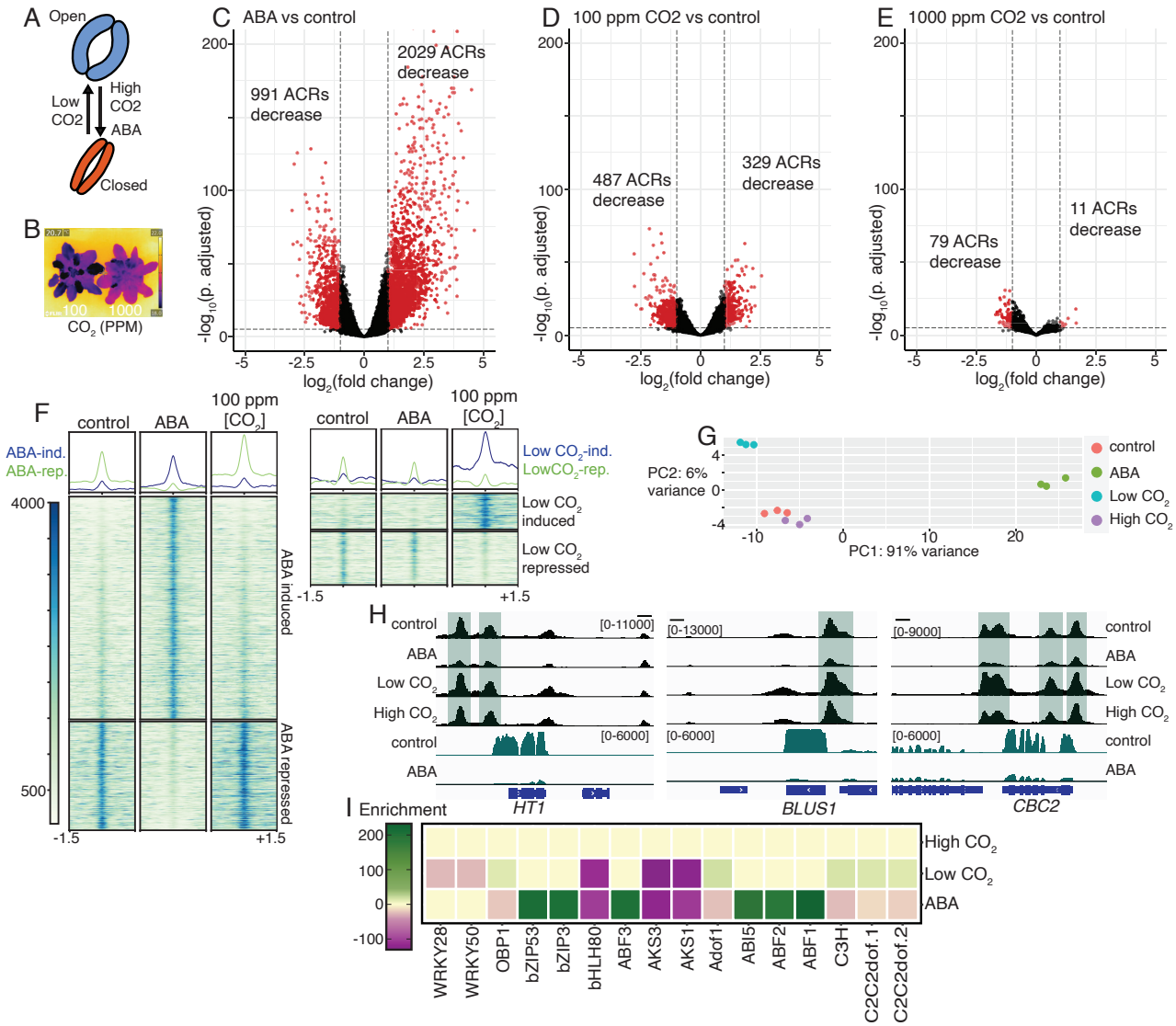

Fig 5. ABA and changes in CO_2 concentration induce distinct chromatin remodeling programs in guard cells. A) Diagram showing the effects of different stimuli on the stomatal aperture. **B)** Representative IR image showing differences in leaf temperature due to CO_2 induced stomatal movement. **C-E)** Volcano plots of ATAC-seq data showing **C)** ABA-regulated chromatin accessibility, **D)** low CO_2 regulated chromatin accessibility, and **E)** high CO2 regulated chromatin accessibility. The number of differentially accessible peaks (colored in red, FDR < 0.001 and FC > 2.0) in each condition is indicated on each plot. **F)** Heatmaps and profile plots of guard cell ATAC-seq signal centered over either ABA-regulated ACRs (2028 induced and 991 repressed) or low CO_2-regulated ACRs (329 induced and 487 repressed). Libraries are derived from plants exposed to the indicated treatments. **G)** Principal component analysis (PCA) shows that ABA, low CO_2, and high CO_2 introduce separate variation to genome-wide chromatin accessibility. **H)** Genome browser snapshots showing ABA-repression of chromatin accessibility upstream of HT1, BLUS1, and CBC1 – three positive regulators of low CO_2 induced stomatal opening. **I)** Enrichment (-log P_value) of the indicated transcription factor binding motifs in ABA, Low CO_2, or High CO_2 regulated regions. Negative enrichment scores indicate motifs overrepresented in condition-repressed regions.

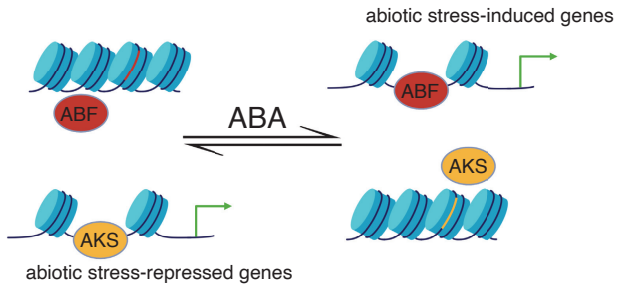

Fig. 6 Model - ABA regulates opposing chromatin states in guard cells. In unstressed guard cells, AKS proteins maintain open chromatin at ABA-repressed genes while ABA-induced genes are kept silent by closed chromatin at their upstream regulatory regions. During abiotic stress, SnRK2s activate ABFs and inhibit AKSs. This leads to the establishment of open chromatin at stress-activated genes and the silencing of ABA-repressed genes by the closing of chromatin. Graphic created with Biorender.com.